Magnetic Properties of Organic Molecular Crystals via an Algebraic Heisenberg Hamiltonian. Applications to WILVIW, TOLKEK, and KAXHAS Nitronyl Nitroxide Crystals

Mercè Deumal,*,† Michael J. Bearpark,† Juan J. Novoa,‡ and Michael A. Robb*,†

Chemistry Department, King's College London, Strand WC2R 2LS London, U.K., and Departament de Química Física, Universitat de Barcelona, Martí i Franquès 1, E-08028 Barcelona, Spain

Received: July 19, 2001; In Final Form: November 4, 2001

A computational approach to the study of magnetism in molecular crystals is outlined, and applications are presented for three purely organic nitronyl nitroxide (NN) crystals: WILVIW (*p*-*N*-methylpyridiniumNN^{+}·I^{-}), TOLKEK (α-2-hydroNN), and KAXHAS (*β*-*p*-nitrophenylNN). Data from ab initio electronic structure computations are used to parametrize an algebraic Heisenberg Hamiltonian. The magnetic susceptibility as a function of temperature $\chi(T)$ is, in turn, obtained directly from the computed energy levels of the algebraic Heisenberg Hamiltonian. The parametrization of the two site interaction parameters J_{AB} requires the identification of the (one-, two-, or three-dimensional) magnetic motifs (e.g., spin ladders, etc.) from a study of the magnetic structure of the crystal. The energy levels of the magnetic motif are then computed as a function of the extension of the constituent magnetic building blocks along the crystallographic axes until convergence on $\chi(T)$ can be demonstrated. Rapid convergence has been demonstrated, showing that a simple model (the minimal magnetic model space) can be used as a realistic model of the magnetic motif for an infinite crystal lattice. Applications to the three organic NN crystals have demonstrated the efficacy of this theoretical approach for the simulation of the experimental magnetic susceptibility and heat capacity data.

Introduction

Transition metal molecular magnetism has been the subject of active research for the last few decades.[1] However, the first bulk organic molecular magnets, the *β* phase of the *p*-nitrophenylNN[2] and the carbon cluster C_{60},[3] were not characterized until 1991. Since then, many other purely organic magnets have been successfully synthesized.[4] Nevertheless, the theoretical models used to explain and simulate the behavior of the magnetic susceptibility $\chi(T)$ for organic/transition metal molecular crystals are still very crude.[5] Those models rarely include an explicit dependence of the magnetic response on the geometry of the constituent radicals for a given crystal. Our purpose in this paper is to present a theoretical approach that incorporates data from ab initio computations providing the magnitude of the microscopic magnetic interactions and that is focused on the importance of the magnetic structure of the crystal.

One usually visualizes the geometric structure of a crystal in terms of a three-dimensional array of chemical bonds (intra or intermolecular in nature). The packing of the constituent building molecules of the crystal can then be described in terms of structural motifs according to the intermolecular bond strength (e.g., electrostatic interactions, hydrogen bonds, Van der Waal forces, etc.). Analogously, the magnetic structure of a crystal can be defined in terms of the topography of a three-dimensional array of dimeric exchange interactions J_{AB} between (radical) sites A and B. The dominant interactions J_{AB} define the constituent magnetic building block of a given crystal. The infinite repetition in one, two, or three directions of the constituent magnetic building blocks defines, in turn, the structure of the magnetic motifs. Finally, the magnetic structure of a crystal for a low-dimensional magnet is defined as an array of infinite-dimensional magnetic motifs, the magnetic interaction between magnetic motifs being sufficiently weak that it can be neglected (see discussion for WILVIW and TOLKEK). For the case of a bulk magnet, the magnetic motif is three-dimensional and coincides with the magnetic structure (see discussion for KAXHAS).

SCHEME 1

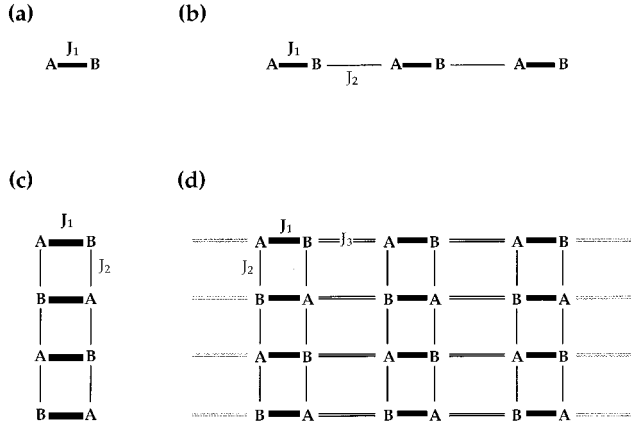

The preceding ideas of magnetic structure at a microscopic level can be illustrated with an example. Scheme 1 shows (a) dimer, (b) linear chain, (c) spin ladder, and (d) two-dimensional layer magnetic motifs. Let us assume that an array of non-interacting two-dimensional layers (Scheme 1d) represents the magnetic structure of a crystal. For $J_1 > J_2 \gg J_3$, the constituent magnetic building block corresponds to a rung (Scheme 1a) and

† King's College London.
‡ Universitat de Barcelona.

10.1021/jp015512u CCC: $22.00
Published on Web 01/25/2002

the magnetic motif becomes a spin ladder (Scheme 1c). Each one of the two-dimensional layers (Scheme 1d) can then be pictured as spin ladders (Scheme 1c) weakly interacting through J_3.

The main goal of this work is to show how the microscopic magnetic motif (chains, ladders, etc.) of the crystal can be related to the macroscopic properties that can be measured, such as magnetic susceptibility and heat capacity. The magnetic structure is not obvious from the crystal structure, and simple models such as the way McConnell's theory is currently applied have been discredited.[6] As we shall show, an objective procedure for connecting the microscopic to the macroscopic magnetic information involves four steps. (1) The identification of all possible magnetic interactions J_{AB} on the basis of intersite A−B distances in the crystal and subsequent computation of the magnitude of the corresponding J_{AB} to determine the dominant contributions (via electronic structure methods such as embedded cluster[7,8] or periodic methods[9]). (2) The pattern and strength of the dominant interactions J_{AB} are then used to define the magnetic building blocks and the magnetic motif, which specifies the magnetic structure of the crystal. (3) The electronic energy levels of the model defined by a finite number of magnetic building blocks of the magnetic motif are then obtained by diagonalization of an algebraic representation of a Heisenberg Hamiltonian parametrized with the computed J_{AB}:

$$\hat{H} = -2\sum_{A,B}^{N} J_{AB}\hat{S}_A\cdot\hat{S}_B \qquad (1)$$

In eq 1, A and B are spin $^1/_2$ sites representing the constituent N radical sites of the magnetic building blocks. This Hamiltonian is then of finite dimension and acts on the space of all possible spin functions that can be constructed from these spin $S = {}^1/_2$ sites. The choice of the number of magnetic building blocks of the magnetic motif to be used in the Heisenberg Hamiltonian (minimal magnetic model space) is a crucial step in this prescription. (4) Finally, the microscopic energy levels obtained by diagonalization of the Heisenberg Hamiltonian are used in standard statistical mechanics methods to give the macroscopic magnetic susceptibility and heat capacity (for a recent review of steps 3 and 4, see ref 10).

A few related theoretical approaches have been documented.[10−12] Borrás-Almenar et al.[10] propose a more general Heisenberg Hamiltonian approach to study magnetic inorganic clusters based on a generalized spin Hamiltonian. However, there is no explicit account of the crystal geometry (except in a parametric form[10,13b−k]) since the J_{AB} values are never numerically computed. Fink et al.[11] use a finite-size cluster approach to compute the energy levels of only the four lowest-lying spin states for binuclear complexes and then calculate $\chi(T)$. We will show that all energy levels seem to be essential in the computation of $\chi(T)$. Hellberg et al.[12] compute $\chi(T)$ by solving the Heisenberg Hamiltonian using Lanczos techniques on large (20−32 spins) clusters to obtain the lowest/highest energy levels and then assume an analytical density of states for the middle eigenvalues. The full four-step prescription given above does however not seem to have been fully tested. Rather, theoretical work often stops at the computation of the J_{AB} for organic and inorganic systems.[7−8] The full Heisenberg Hamiltonian is usually not constructed (except for cluster models[14]), and thus, there is no direct comparison with experiment.

Experimental $\chi(T)$ data are frequently fitted using a Bleaney and Bowers two-level model[15] given by eq 2 (or other analytical expressions[13]):

$$\chi = \frac{2Ng^2{\mu_B}^2}{k_BT}\mu_0\frac{1}{3+\exp(-2\mathbf{J}/k_BT)}\ [\text{emu mol}^{-1}] \qquad (2)$$

Equation 2 can be rigorously derived[16] using the statistical mechanics expression for a two-level model. In this case, there are only two accessible energy levels of the system: the singlet S ground state and the triplet T first excited state. Accordingly, $2\mathbf{J}$ is the S−T spin energy gap of the system. This is clearly only applicable for an antiferromagnetic system (a "two-level" model cannot possibly describe a ferromagnet as will be shown for KAXHAS). The **J** parameter is often erroneously identified with a single type of dimeric interaction J_{AB}. However, a crystal will have more than one type of dimeric interaction. Thus, the **J** parameter in eq 2 effectively "averages" all possible microscopic J_{AB} in the crystal. By "averaging", one means using all magnetically relevant J_{AB} in the parametrization of the Heisenberg Hamiltonian (eq 1) and then solving the secular equation problem for the accessible singlet and triplet states and using only these two levels in $\chi(T)$. The use of two-level models is assumed in many studies published in the literature without numerical justification. In this work, these assumptions will be tested. A least-squares fitting procedure is normally used to reproduce the experimental $\chi(T)$ values using an equation of the form of eq 2 or similar.[17] However, the microscopic magnetic picture that underlies the "best-fitting" model is not available because one obtains an energy difference rather than the individual magnetic J_{AB} interactions. As we shall show, a two-level model (eq 2) can reproduce the experimental $\chi(T)$ values (see discussion for TOLKEK). However, this is not obvious. When the system deviates from this two-level (spin-gap) model (see discussion for WILVIW), the introduction of some empirical factors (e.g., mean field θ parameter) becomes necessary to describe properly the magnetism of the system. These empirical parameters correct the fact that a many-level model is required (the spin-gap model fails). It is thus evident that a theory that incorporates all the microscopic J_{AB} parameters (e.g., using the computed energy levels of a Heisenberg Hamiltonian) is required to relate the microscopic magnetic information J_{AB} to the macroscopic magnetic susceptibility $\chi(T)$.

In summary, we propose a four-step prescription involving: (1) identification and computation of the numerical values of J_{AB}, (2) definition of the magnetic building block, magnetic motif, and magnetic structure, (3) construction and diagonalization of the Heisenberg Hamiltonian, and (4) computation of the macroscopic magnetic susceptibility and heat capacity from statistical mechanics. In the following sections, we will discuss each step, and the methodology involved in it will be compared to the current approaches used by others. Finally, we will present three examples of nitronyl nitroxide crystals where this procedure has been applied.

Theoretical Development

Identification and Computation of the Numerical Values of J_{AB}. The simulation of $\chi(T)$ requires the identification of the magnetic building block of the magnetic motif, which is in turn specified according to the magnitude of the dominant J_{AB}. Therefore, we will proceed to discuss the identification and computation of the numerical values of J_{AB}.

First, the crystal packing must be analyzed. One must identify the potentially important dimeric interactions J_{AB} that exist between the radicals within the asymmetric crystallographic unit cell and those of neighboring crystal cells. Crystals are periodic systems, so the number of unique J_{AB} one needs to identify is

SCHEME 2

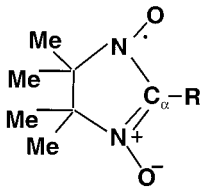

p-N-methylpyridiniumNN$^+$I$^-$, WILVIW R = 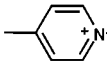 I$^-$

2-hydroNN, α phase , TOLKEK R = — H

p-nitrophenylNN, β phase , KAXHAS R = 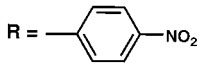

finite. The distance between spin carrier groups in these radicals is the criterion used to decide whether a pair of radicals A−B might be magnetically relevant. Thus, the candidates for dimeric interactions J_{AB} are chosen according to a given cutoff distance between spin carriers since the magnetic interaction is known to vary as $\exp(-r)$ depending on the distance r between magnetic centers and their relative orientation.[18a] Constituent radicals of different crystals belonging to the same family will have the same cutoff distance. One does not assume any preconceived microscopic exchange paths. Rather, one computes the J_{AB} values for all sensible dimeric interactions. The distance criterion per se does not determine the relevant exchange pathways; rather, it provides the initial candidates for the subsequent computation of the J_{AB} values (i.e., we deliberately include more candidates than the first nearest neighbors, which are the usual candidates in the literature). After the identification of the pairs of spin sites, computations are carried out on the whole radical at the geometry of the molecules in the X-ray structure[19] accounting for the relative orientation of the radicals.

The target crystals studied in this paper belong to the nitronyl nitroxide (NN) family (see Scheme 2). These three compounds are characterized by the presence of one unpaired electron in the constituent radical that is mostly localized on the ONCNO unit.[20] Thus, we take the ONCNO atoms as the spin carrier group (the total number of unpaired electrons for a given NN radical depends on the substituent R attached to the α-C of the NN group). For crystals belonging to the NN family, all J_{AB} are computed using the X-ray geometry of pairs of radicals with a spin carrier intersite threshold ONCNO···ONCNO distance of 7.4 Å (at larger distances, the magnetic interaction is assumed to be negligible because of the exponential decay of J_{AB} with distance[18]).

We now turn to the computation of the J_{AB}. Methods such as embedded cluster approach[7,8] or periodic methods[21] have been used in order to compute the magnitude of J_{AB}. A "dressed" cluster approach would be required for transition metal crystals, where one takes into account the cluster and its environment.[7] However, a "bare" cluster approach is adequate for organic crystals. Thus, in the computation of J_{AB} values, we use standard electronic structure computations for the singlet−triplet energy separation using unrestricted DFT with broken symmetry.[22]

Some practical aspects of the computation of J_{AB} within the unrestricted DFT broken symmetry approach[22] are now discussed. From the Heisenberg Hamiltonian (eq 1) for a pair of radicals A and B with one unpaired electron, the J_{AB} value is computed as the energy difference between biradical open-shell singlet S and triplet T states

$$\Delta E^{S-T} = E^S - E^T = 2J_{AB} \tag{3}$$

When using DFT, the use of the unrestricted broken symmetry approach is required in order to compute the biradical open-shell singlet ground state. From a variety of choices,[22] the criteria followed to compute the energy difference is

$$E^S - E^T = \frac{2(E^S_{BS} - E^T)}{1 + S_{ab}{}^2} \tag{4}$$

where S stands for singlet, T for triplet, and BS for broken symmetry and S_{ab} is the overlap integral between a and b singly occupied molecular orbitals (SOMOs). For all three NN crystals studied in this paper, the solutions for the biradical open-shell singlet have localized SOMOs on one radical or on the other, so the overlap is negligible ($S_{ab} = 0$). Thus, eq 4 becomes simply

$$E^S - E^T = 2(E^S_{BS} - E^T) \tag{5}$$

and

$$E^S_{BS} - E^T = J_{AB} \tag{6}$$

We have used unrestricted DFT, with the UB3LYP[23] functional using broken symmetry, and a 6-31+G(d) basis set[24] (Gaussian package[25]).

It is clear that the bare dimer approach neglects three-, four- or *n*-body cooperative exchange effects. Depending on the substituent R attached to the α-C of the NN group (see Scheme 2), these many-body effects may be large (R = phenyl group) or small (R = hydrogen atom). Other more accurate ab initio methods (e.g., FCI, CC, DDCI, CASPT2...[26]) could be used to compute the exchange coupling J_{AB} whenever the size of the system allows it. However, we shall show that it is the topography of the magnetic motif of the crystal that is important when simulating $\chi(T)$ rather than the accuracy of the computed J_{AB}. Once the topography of the J_{AB} has been identified, we will show that $\chi(T)$ can be fitted by uniform scaling of all the computed J_{AB}.

Definition of the Magnetic Building Block, Magnetic Motif and Magnetic Structure. The magnitude of the dominant dimeric exchange interactions J_{AB} (computed as described in previous section) defines the magnetic building block of the crystal. The magnetic motif is then defined by the infinite appropriate repetition of this magnetic building block, which is first extended along the direction given by the largest J_{AB}, then along the direction of the second largest J_{AB}, and so on. Scheme 1 shows the topography of four different magnetic motifs in terms of J_1, J_2, J_3... between radicals A and B: (a) dimer, (b) linear chain, (c) spin ladder, and (d) two-dimensional layer. The relative ratios between computed J_{AB} values define different motif topographies in terms of magnetic building blocks.[27] Therefore, the correct definition of the magnetic building block is essential to properly represent the microscopic magnetic topography. The extension of the number of magnetic building blocks in terms of J_{AB} is carried out according to the topography of J_{AB} and not according to the repetition of crystallographic cells of the crystal. For instance, assuming $J_3 \ll J_1$ and J_2, Scheme 1d shows an array of non interacting spin ladders (Scheme 1c). In such a case, a spin ladder is the magnetic motif providing all the relevant microscopic information. In contrast, the broken lines in Scheme 1d represent a crystallographic unit

cell containing a pair of radicals A and B. It follows that the repetition of this unit cell is not related to the magnetic motif.

Finally, the magnetic structure of the crystal is defined according to the infinite repetition of a given magnetic motif. Using the above example, if the magnetic motif for a crystal is a spin ladder (Scheme 1c), the three-dimensional magnetic structure is formed by infinite noninteracting (or very weakly interacting) spin ladders. For the special case of bulk magnets (the magnetic motif is three-dimensional), the magnetic structure and the magnetic motif coincide (as illustrated with KAXHAS).

Construction and Diagonalization of a Heisenberg Hamiltonian. The simulation of macroscopic properties, such as magnetic susceptibility $\chi(T)$ and heat capacity $C_p(T)$, is carried out using the energy levels obtained from the diagonalization of a Heisenberg Hamiltonian. This Hamiltonian is, in turn, parametrized with the previously computed J_{AB}. The magnetic motif (for a finite number of magnetic building blocks) defines the dimension of the Heisenberg Hamiltonian. Thus, from a practical viewpoint, the concept of magnetic motif (and in particular the constituent magnetic building block) enables one to reduce the problem of an infinite crystal into a finite model (i.e., it enables the use of a Heisenberg Hamiltonian).

For organic molecular crystals, the energy levels are obtained from the full numerical solution of the secular equation problem of the algebraic Heisenberg Hamiltonian given by eq 1, which is rewritten as[28]

$$\hat{H} = -\sum_{A,B}^{N} J_{AB}(2\hat{S}_A \cdot \hat{S}_B + {}^1/_2\hat{I}_{AB}) \qquad (7)$$

In eq 7, the sum A and B runs over a subset of N magnetic $S = {}^1/_2$ centers of the magnetic motif for a finite number of constituent magnetic building blocks. $\hat{S}_A$ is the spin operator associated with the radical A, and $\hat{I}_{AB}$ is the identity operator. The J_{AB} are the microscopic parameters which give the magnetic exchange coupling interaction between those centers (computed as described previously). If J_{AB} is negative, the spins within the radical site pair tend to be antiparallel to each other (antiferromagnetic coupling), while if J_{AB} is positive, the spins align parallel to each other (ferromagnetic coupling). The Hamiltonian (eq 7) operates on a basis of N-fold tensor products consisting of products of N spins (either α or β for a system of doublets) in the crystal.[29]

The space of Heisenberg Hamiltonian (eq 7) is defined by the choice of a finite number of magnetic building blocks of the magnetic motif.[29] However, the choice of the number of building blocks to be used in the construction of the Hamiltonian remains to be discussed. One must demonstrate convergence on $\chi(T)$ with respect to the extension of the number of magnetic building blocks (according to the topography of the magnetic motif). As we will show subsequently, rapid convergence can be demonstrated indicating that simple models with small number of magnetic centers (4−8 radical sites) may be adequate to provide a realistic model of the magnetic motif for an infinite crystal lattice. Thus, the only practical limit, from a computational point of view in our approach, is the restriction to about 16 radical sites because of the need to fully diagonalize the Hamiltonian (with 16 active sites, H in eq 7 has a dimension of 12870 by 12870). However, two conceptual issues remain: (1) whether to simulate the magnetic motif with an open or cyclic model, and (2) an a priori rationalization of the reason small models may provide a rapid convergence on the computed magnetic susceptibility $\chi(T)$ data.

Calculations have been carried out on a series of large finite cyclic chains.[30,31a] It is believed that the properties of an infinite chain of atoms can be properly reproduced by a finite cyclic chain (less than 30 atoms is enough in many cases[30]). The same approach can be extrapolated to three-dimensional problems. However, an open cluster approach[31] is also possible. If a particular property of the cluster has converged, the limiting value is considered as that of the infinite system; otherwise, an estimation of the bulk-limit results can be done.[31] A series of tests using open and cyclic models corresponding to the extension of the number of magnetic building blocks has been carried out for the three crystals studied in this paper. The results obtained using all energy levels computed for both models show quasi-identical $\chi(T)$ curves (we will just show the results for WILVIW).

SCHEME 3

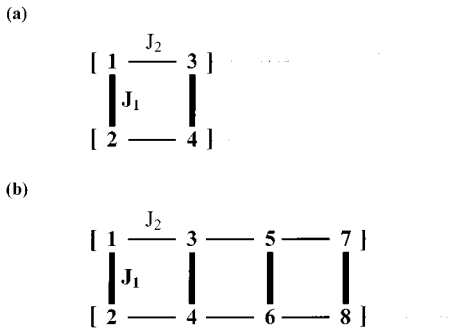

Effective Hamiltonian theory[32] can be used to understand and demonstrate the rapid convergence of the simulated magnetic susceptibility data using simple models. This methodology has been tested to be valid for a number of spin problems.[33] The use of an effective Hamiltonian[32,33] requires the introduction of two new concepts, minimal magnetic model space and target space, which we will illustrate with an example. Scheme 1c shows a spin ladder magnetic motif. For such a magnetic motif, the magnetic building block (mbb) could be pictured as a dimer (rung) assuming a dominant J_1 interaction. A 2mbb model (4-spin sites in Scheme 3a) could be thought as being the minimal magnetic model space for a 4mbb target space (8-spin sites in Scheme 3b) since the latter is a double repetition. In such a case, the diagonalization of the Hamiltonian using the 4mbb model, and its subsequent projection onto the 2mbb space will yield six eigenstates (out of 70 eigenvectors corresponding to the 4mbb target space) matching the six eigenstates of the 2mbb minimal magnetic model space (a quintet, three triplet and two singlet states). If the computed $\chi(T)$ data do not change when increasing the size of the target space (4-, 5-, *n*-mbb model) while keeping the same minimal magnetic model space (2mbb model, onto which the target space Hamiltonian is projected), the calculation is converged (see discussion for WILVIW crystal). One then also concludes that the minimal magnetic model space can provide a faithful representation of the infinite system.

Within the framework of effective Hamiltonian theory, instead of working with the Hamiltonian of the infinite crystal space, one uses its projection onto a subspace of magnetic building blocks. This subspace is the smallest subset of magnetic building blocks required to describe properly $\chi(T)$, the so-called minimal magnetic model space. The space of the effective Hamiltonian is thus the minimal magnetic model space. The space defined by a larger number of magnetic building blocks is in turn called the target space. The effective Hamiltonian[33] projected from a target space will always reproduce exactly a subset of eigenvalues of this target space corresponding to the minimal magnetic model space. The accepted strategy for the study of

periodic systems, using finite models, involves the systematic extension of the finite system until convergence is obtained. Thus, we have used this strategy by extending the minimal magnetic model along the crystallographic directions until we obtain convergence.

Macroscopic Magnetic Susceptibility and Heat Capacity from Statistical Mechanics. Once the microscopic information has been obtained (J_{AB} values) and the energy levels of the Heisenberg Hamiltonian computed, one can simulate the magnetic susceptibility and heat capacity using statistical mechanics. The behavior of $\chi(T)$ shows whether the molecular material behaves macroscopically as a ferro or antiferromagnet. Experimentally, susceptibility measurements are conducted at very low magnetic fields to avoid saturation effects in the magnetic data (e.g., using SQUID[34]). Thus, the expression for $\chi(T)$ will be derived at zero magnetic field B limit.

The general expression for the magnetic susceptibility $\chi(T)$ given by statistical mechanics is written in terms of the microscopic energy levels at zero magnetic field as[5]

$$\chi = \frac{Ng^2{\mu_B}^2}{k_B T}\mu_0\left[\frac{\sum_n \sum_{m_{S_n}=-S}^{+S} (m_{S_n}+S_0)^2 \exp\left[-\frac{E_n-E_0}{k_B T}\right]}{\sum_n (2S_n+1)\exp\left[-\frac{E_n-E_0}{k_B T}\right]} - \frac{\left[\sum_n \sum_{m_{S_n}=-S}^{+S} (m_{S_n}+S_0)\exp\left[-\frac{E_n-E_0}{k_B T}\right]\right]^2}{\left[\sum_n (2S_n+1)\exp\left[-\frac{E_n-E_0}{k_B T}\right]\right]^2}\right] \quad (8)$$

The above expression can further reduce to[35]

$$\chi = \frac{Ng^2{\mu_B}^2}{3k_B T}\mu_0\left[\frac{\sum_n S_n(S_n+1)(2S_n+1)\exp\left[-\frac{E_n-E_0}{k_B T}\right]}{\sum_n (2S_n+1)\exp\left[-\frac{E_n-E_0}{k_B T}\right]}\right] \quad (9)$$

after summing over m_{S_n} (at zero magnetic field limit). Similarly, the statistical mechanics expression for the heat capacity $C_p(T)$ in terms of the microscopic energy levels is

$$C_p = \frac{N}{k_B T^2}\left[\frac{\sum_n (2S_n+1)(E_n-E_0)^2 \exp\left[-\frac{E_n-E_0}{k_B T}\right]}{\sum_n (2S_n+1)\exp\left[-\frac{E_n-E_0}{k_B T}\right]} - \frac{\left[\sum_n (2S_n+1)(E_n-E_0)\exp\left[-\frac{E_n-E_0}{k_B T}\right]\right]^2}{\left[\sum_n (2S_n+1)\exp\left[-\frac{E_n-E_0}{k_B T}\right]\right]^2}\right] \quad (10)$$

In the above expressions, E_n is the nth energy level from the algebraic Heisenberg Hamiltonian, S_n is the spin of the nth energy level ($m_{S_n} = -S_n, ..., -1, 0, +1, ..., +S_n$), g is the gyromagnetic factor, and the constants N, μ_B, k_B, and μ_0 are Avogadro's number, Bohr magneton, Boltzmann constant, and permeability of free space, respectively. The units of χ (eq 9) in SI are $m^3\ mol^{-1}$ dimers (and in CGS system, $\chi/4\pi 10^{-6}$ gives the susceptibility in emu mol^{-1} dimers).[36] The units for C_p (eq 10) are J mol^{-1} K^{-1}. It is thus essential to clarify whether "mol^{-1}" in N refers to moles of magnetic centers (radicals), pairs of radicals (dimers), minimal magnetic model space, etc. The units of the energy E_n must then be in accordance with N and refer to a mole of radicals, dimers, minimal magnetic model space, etc.

Two strategies can be followed when computing the magnetic susceptibility (eq 9) as a function of temperature $\chi(T)$, depending on whether the energy levels are obtained using (1) the Heisenberg Hamiltonian in the target space or (2) its projection onto a model space. A Heisenberg Hamiltonian is applied to different target spaces with increasing number of magnetic building blocks until convergence on $\chi(T)$ is obtained. It is essential that all the energy levels $\{E_n\}$ and corresponding spin values $\{S_n\}$ from each target space are included in the statistical mechanics expression (9) (e.g., ref 11 only uses the 4 lowest spin states for a binuclear complex). However, the projection of the Heisenberg Hamiltonian onto the minimal magnetic model space via an effective Hamiltonian reproduces a subset of eigenvalues of a target space and can be used as well. When working with the projected Heisenberg Hamiltonian, only the energy levels $\{E_n\}$ and corresponding spin values $\{S_n\}$ of the minimal magnetic model space are included in the statistical mechanics expression. If the computed $\chi(T)$ does not change when increasing the size of the target space (keeping the same minimal magnetic model space), the calculation (eq 9) is converged. We will exemplify both strategies in the following section. Once the $\chi(T)$ data have been computed using the energy levels of either Hamiltonian, comparison to the experimental values is always carried out.

Let us now digress to compare our approach with the standard solid-state approach to the quantum mechanical modeling of an infinite periodic system. CRYSTAL package[21] is the periodic ab initio program often applied to magnetism-related problems. In CRYSTAL, the energy of an infinite crystal is computed using the Hartree−Fock (or Kohn−Sham) formalism within the LCAO approximation. An a priori choice of the magnetic unit cell and spin configuration has to be made. Then the UHF (UDFT) energy is obtained for this local minimum using this specific electronic configuration as a starting guess (i.e., preassigning a spin arrangement within the magnetic unit cell). The process is then repeated for some spin arrangements. The microscopic magnetic exchange J_{AB} parameters for these particular configurations[37,38] are obtained from the computed energies for the various spin arrangements by solving the relevant equations involving the diagonal matrix element symbolic expressions for the Heisenberg Hamiltonian (for an analogous treatment see ref 12). However, the computation of all the energy levels required in the expression of $\chi(T)$ is not carried out. In principle, the J_{AB} values obtained with CRYSTAL could be reintroduced in an algebraic Heisenberg Hamiltonian to compute the energy levels required for the statistical mechanics computation of $\chi(T)$. Hellberg et al.[12] have obtained the magnetic exchange vanadium−vanadium coupling J_{V-V} for CaV_4O_9 from the energy of seven different configurations using a periodic method equivalent to CRYSTAL based on plane waves. The authors have followed the former prescription to compute the energy levels by solving the Heisenberg Hamil-

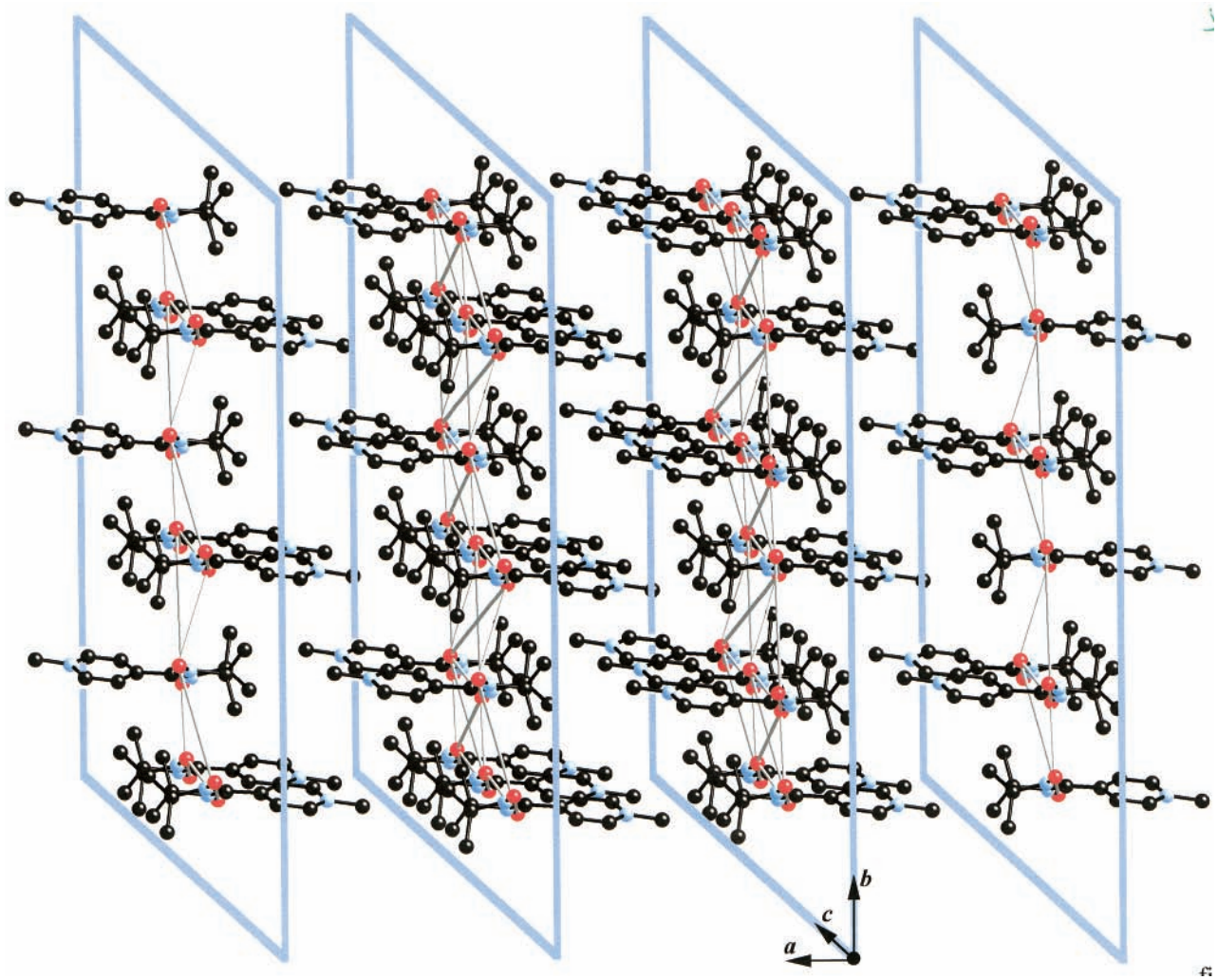

Figure 1. Snapshot of the magnetic structure for WILVIW crystal (hydrogen atoms are not shown, see Scheme 2 for radical formula). WILVIW radicals with ONCNO···ONCNO distance shorter than 7.4 Å are connected with a line. The connected radicals form a two-dimensional layer that extends along *bc* crystallographic axes. The infinite stack of parallel noninteracting two-dimensional layers along the *a* crystallographic direction are shown (distance between two neighboring layers is larger than the cutoff of 7.4 Å).

tonian with Lanczos techniques on finite (20-spin) periodic clusters using the previously computed J_{V-V}, and then simulating $\chi(T)$.

In addition, several other numerical techniques have been used to study the low-energy properties of strongly interacting quantum lattice models described by a model Hamiltonian accounting for periodic boundary conditions, such as quantum Monte Carlo (QMC[39]) and density matrix renormalization group (DMRG[40]). However, none of them has universal applicability, and so they will not be the subject of further discussion.

Results and Discussion

We will now discuss the results obtained using the preceding four-step prescription for two antiferromagnetic nitronyl nitroxide NN crystals, WILVIW (p-*N*-methylpyridiniumNN^{+}•I^{-}) [41] and TOLKEK (2-hydroNN, α phase)[42], and for the ferromagnetic NN crystal KAXHAS (*p*-nitrophenylNN, β phase)[2] (nomenclature taken from CCSD[43]). Notice that the constituent radicals in these three crystals have just one unpaired electron that is mostly delocalized on the ONCNO atoms (see Scheme 2), which are taken as the spin carrier group. For WILVIW, a detailed discussion will be given on how to identify and compute the numerical values of J_{AB}, determine the magnetic building block, magnetic motif and magnetic structure, construct and diagonalize a parametrized Heisenberg Hamiltonian, and compute the macroscopic magnetic susceptibility from statistical mechanics. However, for TOLKEK and KAXHAS, we will just outline the main results. Full documentation is contained in Supporting Information.

WILVIW. The WILVIW crystal (*p*-*N*-methylpyridiniumNN^{+}• I^{-}; for radical, see Scheme 2) has P1 symmetry with parameters $a = 11.843$ Å, $b = 12.695$ Å, $c = 9.532$ Å, $\alpha = 95.53°$, $\beta = 90.55°$, and $\gamma = 146.89°$. There are two WILVIW radicals per unit cell ($Z = 2$). It is known to be an antiferromagnet.[41] The experimental magnetic susceptibility data have been fitted to a Bleaney−Bowers expression corrected with an empirical mean field θ parameter

$$\chi = \frac{4C}{T[3 + \exp(-2\mathbf{J}/k_B T)] - \theta} \text{ [emu mol}^{-1}\text{]} \qquad (11)$$

where $\mathbf{J}/k_B = -74.0$ K (-51.4 cm^{-1}), $\theta = -4.7$ K (-3.3 cm^{-1}), and $C = 0.376$ emu K mol^{-1}.

First, we proceed by analyzing the packing of the crystal in terms of magnetic interactions. Figure 1 shows the packing of the WILVIW crystal indicating those dimeric interactions J_{AB} between constituent radicals that meet the cutoff criterion[18] and thus might be magnetically important (hydrogen atoms are not

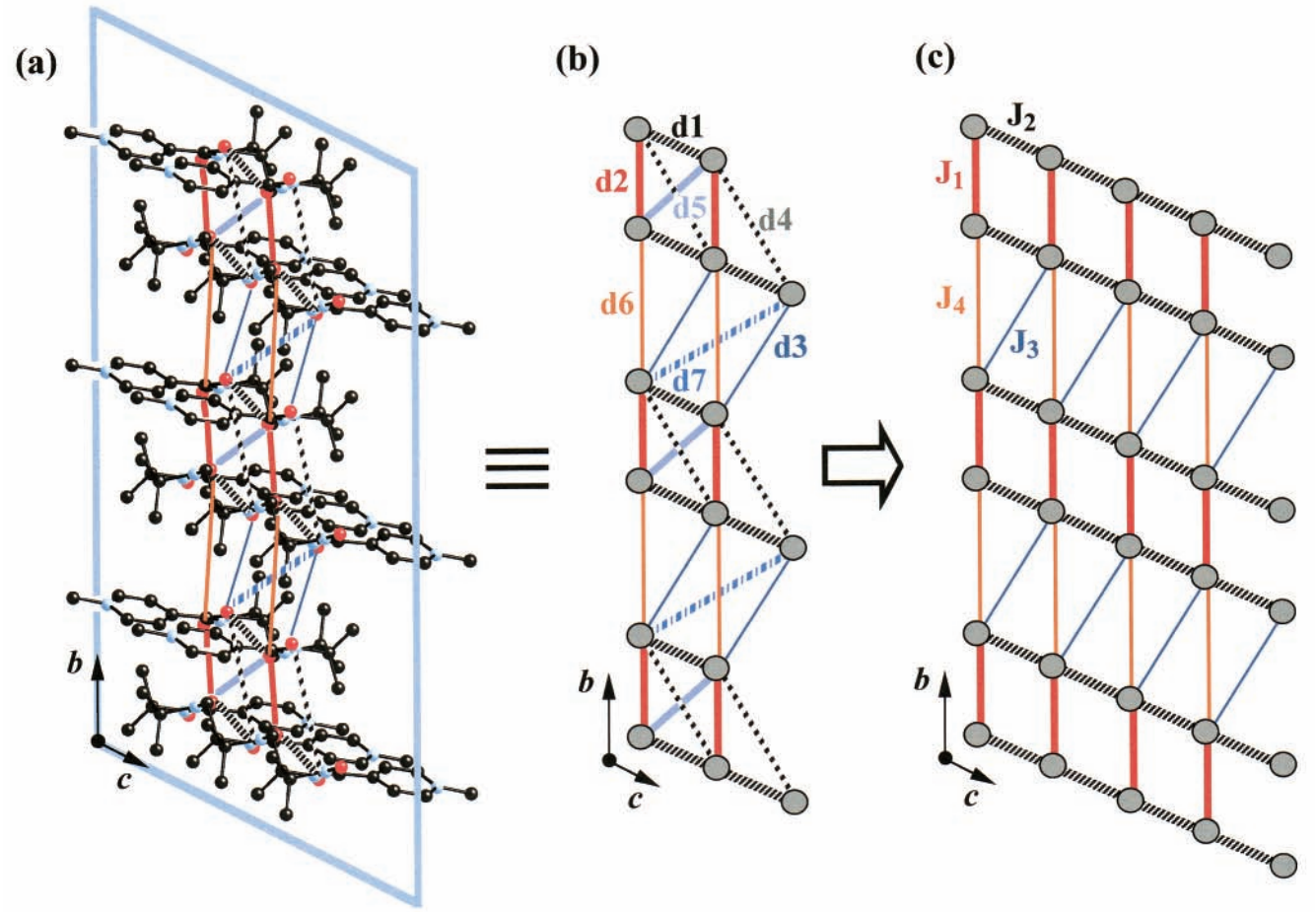

Figure 2. (a) Simplified view of a two-dimensional layer for WILVIW showing the seven pairs of radicals d_i (hydrogen atoms are omitted) with an ONCNO···ONCNO distance shorter than 7.4 Å. Different d_i pairs of radicals are represented diagrammatically with different lines. (b) Schematic view of the topography of the two-dimensional layer (a). Each WILVIW radical is replaced with a point site, and lines are labeled according to the d_i pairs of radicals they connect ($i = 1-7$ with increasing O···O distance). (c) Magnetic motif for WILVIW is defined in terms of nonnegligible J_i dimeric interactions ($i = 1-4$ with decreasing strength) between d_i pairs of radicals. The magnetic motif is a spin ladder defined by J_1 (rungs, i.e., magnetic building block) and J_2 (legs). The two-dimensional layer consists of spin ladders weakly interacting through J_3 and J_4. (Inset in the figure, *bc* crystallographic axes are shown.)

shown; see Scheme 2 for radical formula). Each line connecting two ONCNO groups represents an individual J_{AB} (only one line per pair of radicals). For WILVIW, the magnetic interactions form a stack of parallel two-dimensional layers (*bc* crystallographic directions in Figure 1). We assume these layers do not interact along the *a* crystallographic direction because they are further apart than the cutoff distance of 7.4 Å. Therefore, the magnetic structure for WILVIW is a two-dimensional layer, which is part of a stack of parallel noninteracting layers in the three-dimensional magnetic packing.

Figure 2a shows a simplified two-dimensional layer (hydrogen atoms are omitted), and Figure 2b depicts a schematic view of the topography of this layer. In Figure 2b, each radical molecule is reduced to a point site, and all dimeric interactions J_{AB} less than 7.4 Å are drawn diagrammatically as a line (only one line per pair of radicals). These lines are pictured plain, bold, broken, etc., to distinguish among seven different pairs of radicals (d1−d7 in Figure 2b) that repeat themselves thanks to the $P\bar{1}$ symmetry of the crystal.

Now we discuss the magnitude of the computed dimeric interaction J_{AB} for the seven d1−d7 pairs. Unrestricted broken symmetry UB3LYP/6-31+G(d)[22−25] has been used to compute the J_{AB} values via eq 6 using the geometry of each dimer taken directly from the crystal structure (using CCSD[43]). Table 1 contains the computed dimeric interactions J_i ($i = 1-7$) for d1−d7 (dimers are listed as shortest O···O distance increases). One can see that only four dimeric interactions are magnetically important and will thus contribute to the macroscopic magnetism of the crystal. Interestingly, the strength of the J_{AB} interactions is not proportional to the O···O distance (see Table 1), showing that the relative orientation of the pair of radicals plays an important role. The fourth column in Table 1 gives the ordering of J_1... J_4 relative to the magnetically strongest dimeric interaction.

TABLE 1: Unrestricted DFT Broken Symmetry UB3LYP/6-31+G(d) Results for the Dimeric Interaction of All Seven Candidates (d1−d7 listed as O···O Distance Increases) for WILVIW[a]

candidate *i*	d_i(O···O)/Å	J_i/cm^{-1}	J_i ordering
d1	3.16	−9.1	J_2
d2	3.38	−28.2	J_1
d3	4.37	−1.5	J_3
d4	5.85	< |0.05|	
d5	6.04	< |0.05|	
d6	6.46	+1.1	J_4
d7	6.71	< |0.05|	

[a] The fourth column gives the ordering of the four non-negligible dimeric interactions J_1···J_4 from strongest to weakest dimeric interaction.

The data contained in Table 1 are used to identify the actual magnetic motif for WILVIW in terms of the constituent

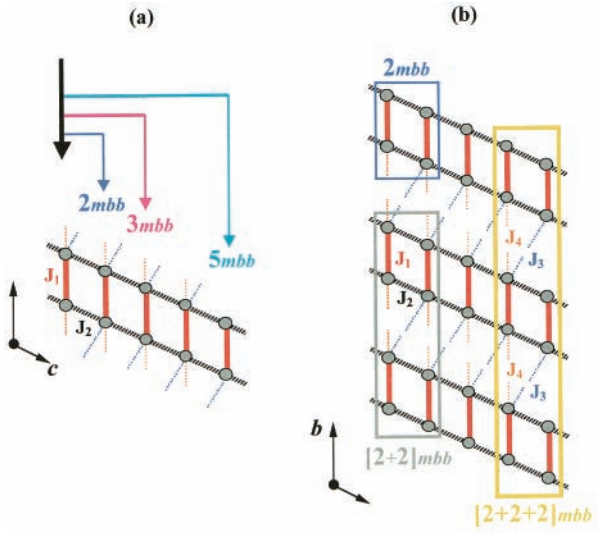

Figure 3. Models used to study the convergence of the macroscopic susceptibility for WILVIW. Extension of the number of magnetic building blocks (mbb) (a) along the *c* axis for an isolated spin ladder from 2 (2mbb) to 5 (5mbb) magnetic building blocks and (b) along the *b* axis for the case of two ([2+2]mbb) and three ([2+2+2]mbb) interacting spin ladder 2mbb models.

magnetic building blocks (mbb). The largest dimeric interaction value ($J_1 = -28.2$ cm^{-1}) defines the magnetic building block as a dimer. This dimer is then replicated along the second largest J_{AB} value ($J_2 = -9.1$ cm^{-1}) (Figure 2c) so that the magnetic motif becomes a spin ladder defined by J_1 (rungs) and J_2 (legs). This spin ladder motif, in turn, interacts weakly with nearby ladders through J_3 and J_4, as shown in Figure 2c. For WILVIW, the magnetic building block of the spin ladder (magnetic motif) is a rung (dimer). Thus, the extension of the number of rungs along the *bc* axes (two-dimensional layer magnetic structure) is the finite model used when applying the algebraic Heisenberg Hamiltonian (eq 7) to compute the microscopic energy levels required by the statistical mechanics definition of the magnetic susceptibility (eq 9). To reproduce the experimental $\chi(T)$ data, one must demonstrate convergence on $\chi(T)$ with respect to the extension of the number of magnetic building blocks (according to the topography of the magnetic motif).

We begin the discussion on the convergence of the macroscopic susceptibility $\chi(T)$ for WILVIW, by increasing the number of rungs (mbb) along the *c* axis for an isolated spin ladder from 2 (2mbb, i.e., a 4-spin site model) to 5 (5mbb, i.e., a 10-spin site model), according to Figure 3a. By extending the number of rungs along the spin ladder, the dimension of the secular equation in the Heisenberg Hamiltonian problem increases from 6×6 (4 spin sites, i.e., a 2 rung (2mbb) model) to 252×252 (10 spin sites, i.e., a 5 rung (5mbb) model). Next, the convergence of $\chi(T)$ is studied extending the magnetic building block along the *b* axis for the case of two ([2+2]mbb) and three ([2+2+2]mbb) interacting spin ladder 2mbb models (Figure 3b).

In Figure 4a, we plot $\chi T(T)$ data computed according to the models shown in Figure 3. A very rapid convergence is achieved by extending the number of rungs along a spin ladder from 2 to 5 (see Figure 3a for model). The discrepancy between simulated and experimental data will be discussed subsequently. Notice that all the simulated $\chi(T)$ curves are almost the same irrespective of the size of the model being used. Tests using a "cyclic" spin ladder model of increasing size also show a complete agreement with the magnetic susceptibility $\chi(T)$ data obtained with an "open" spin ladder model (Figure 5). It

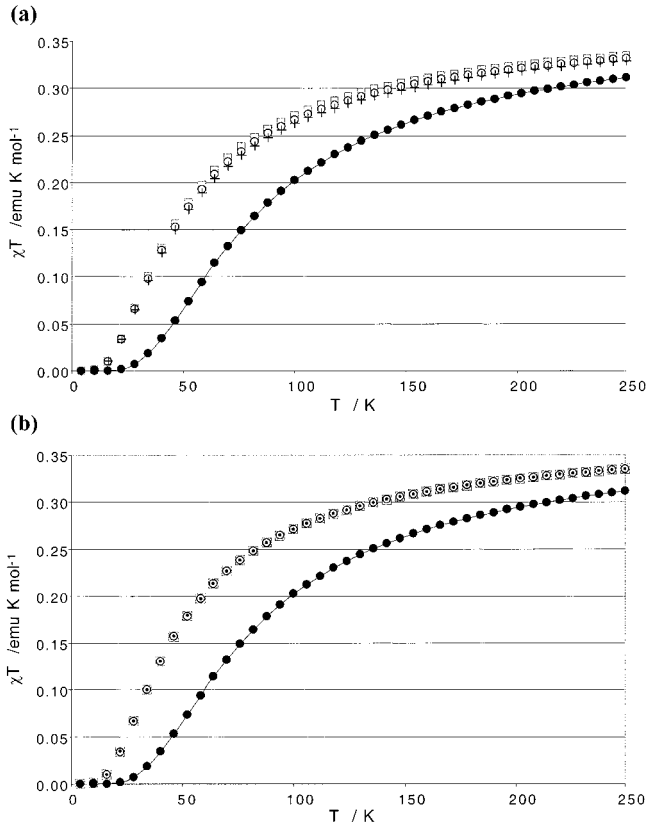

Figure 4. (a) $\chi T(T)$ computed by extending the number of magnetic building blocks along the *c* axis for an isolated spin ladder from 2mbb (■), 3mbb (○), and 5mbb (+) (see Figure 3a for models). (b) $\chi T(T)$ obtained by extending the number of interacting spin ladders from one (2mbb ■), two ([2+2]mbb ○), and three ([2+2+2]mbb ·) (see Figure 3b for models). The experimental data are shown as (●).

follows that the simple 2mbb model seems to be adequate as a minimal model of the infinite spin ladder.

We now allow the spin ladders to interact among themselves to reproduce the magnetism in the *bc* planes of the WILVIW crystal. Now, $\chi(T)$ is simulated using two-interacting ([2+2]-mbb) and three-interacting ([2+2+2]mbb) spin ladder 2mbb minimal models and compared to the computed data for an isolated 2mbb model (Figure 3b). Again, the computed $\chi T(T)$ data using these three models agree (see Figure 4b). Thus, one can conclude that a 2mbb model is the minimal model that describes the magnetic motif for WILVIW. Note also that the 2mbb model is the smallest model containing the two largest J_{AB} dimeric interactions. In fact, Awaga et al.[41] suggested that the dimers with O···O distance of 3.38 and 3.16 Å (J_1 and J_2, respectively, in Table 1) might be responsible for the magnetism of WILVIW.

The use of the projected Heisenberg Hamiltonian enables one to understand why the 2mbb minimal magnetic model space is appropriate for the magnetic motif of WILVIW. The energy levels obtained with the effective Hamiltonian in the minimal magnetic model space (2mbb in Figure 3) reproduce exactly a subset of eigenvalues of a target space that consists of a larger number of magnetic building blocks (3mbb, 4mbb, 5mbb, [2+2]-mbb... in Figure 3). If the computed $\chi(T)$ data do not change when increasing the size of the target space (6-, 8-, 10-, *n*-spin sites model) keeping the same minimal magnetic model space (2mbb model with 4-spin sites) onto which the target space Hamiltonian is projected, the calculation is converged. Figure 6 shows the agreement between the simulated $\chi(T)$ data using the energy levels obtained from the 2mbb minimal magnetic

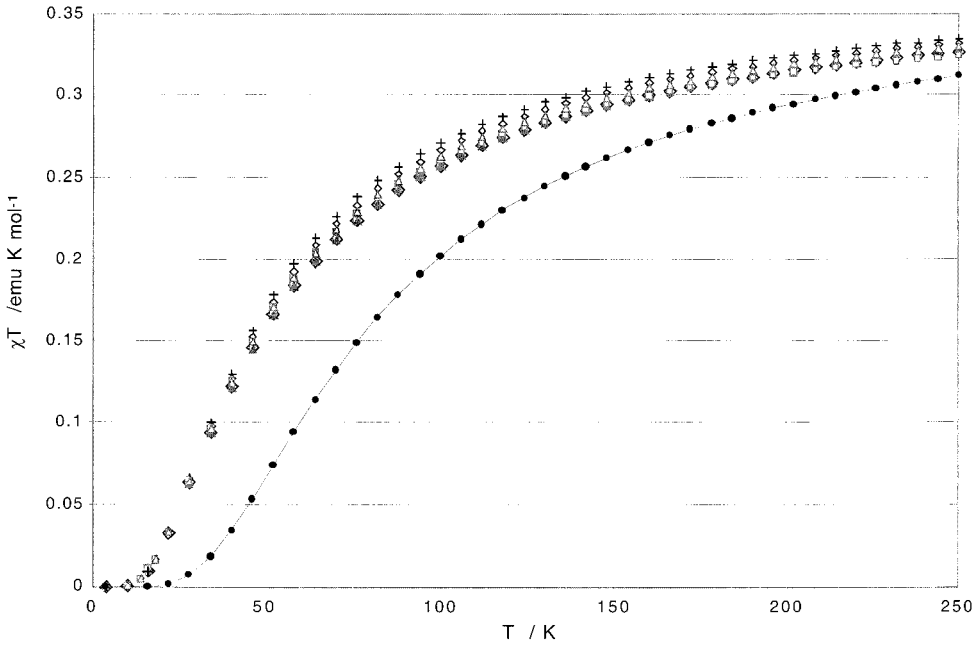

Figure 5. Comparison between the simulated $\chi T(T)$ data using a "cyclic"/"open" spin ladder motif of increasing number of magnetic building blocks for a 3mbb (♦/◇), 4mbb (■/□), and 5mbb (▲/△) models. The 2mbb open model (+) and the experimental data (●) are given as a reference.

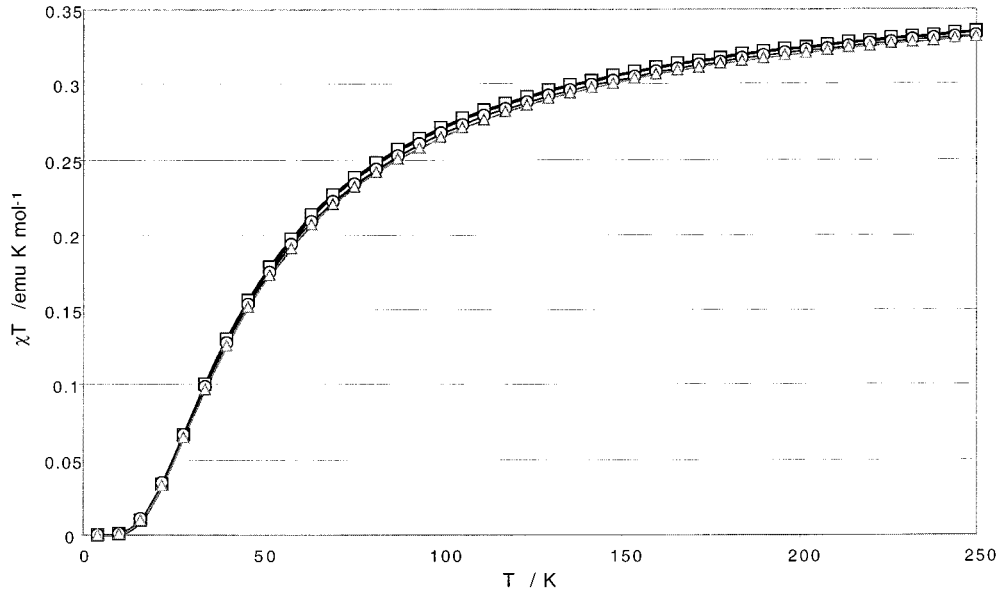

Figure 6. Simulated $\chi T(T)$ data from projected effective Hamiltonians onto the energy levels obtained for the 2mbb minimal magnetic model space (■) and those from the projected 3mbb (○) and 4mbb (▲) target spaces onto the minimal magnetic model space.

model space and those of the effective Hamiltonian obtained from the 3mbb and 4mbb target spaces. It is clear that the calculation is converged.

Let us now discuss the difference between simulated and experimental values that appears in Figure 4. The computed curve clearly has the correct shape, suggesting that the magnetic motif is correct. Thus, a scaling factor multiplying all J_{AB} interactions has been introduced. The scaling factor indirectly accounts for the systematic errors due to computing the microscopic magnetic exchange interactions J_{AB} using DFT[44] and to cooperative exchange effects between different J_{AB}'s, which are neglected when using a bare dimer approach (WILVIW has a pyridinium ring as R substituent attached to the α-C of the NN group, see Scheme 2). In Figure 7a, one can see that applying a scaling factor of 1.6 or 1.7 to the 2mbb model reproduces the $\chi T(T)$ data obtained from experiment. One can discriminate between the two factors by plotting $\chi(T)$ rather than $\chi T(T)$ (Figure 7b), from which it is clear that a scaling factor of 1.7 is more adequate. Note that the scaling factor we use throughout the paper is linear because our target is to reproduce qualitatively the experimental curves, and the use of the same factor for all J_{AB} parameters is the simplest approach one can follow.

Comparison of the singlet−triplet spin-gap for different target spaces (3−5mbb, [2+2]mbb, [2+2+2]mbb, [3+3]mbb projected onto a minimal 2mbb, see Figure 3) shows that it has approximately the same value (-49.8 ± 1.6 cm^{-1} in average) irrespective of the target space being used [Supporting Information Table S1]. The spin-gap for each individual target space decreases as the size of the target space increases, but the projected spin-gap is kept constant [see arrows for projected singlet and triplet states in Supporting Information Figure S1]. The fact that different target spaces converge to the same projected spin-gap is consistent with the 2mbb model being the

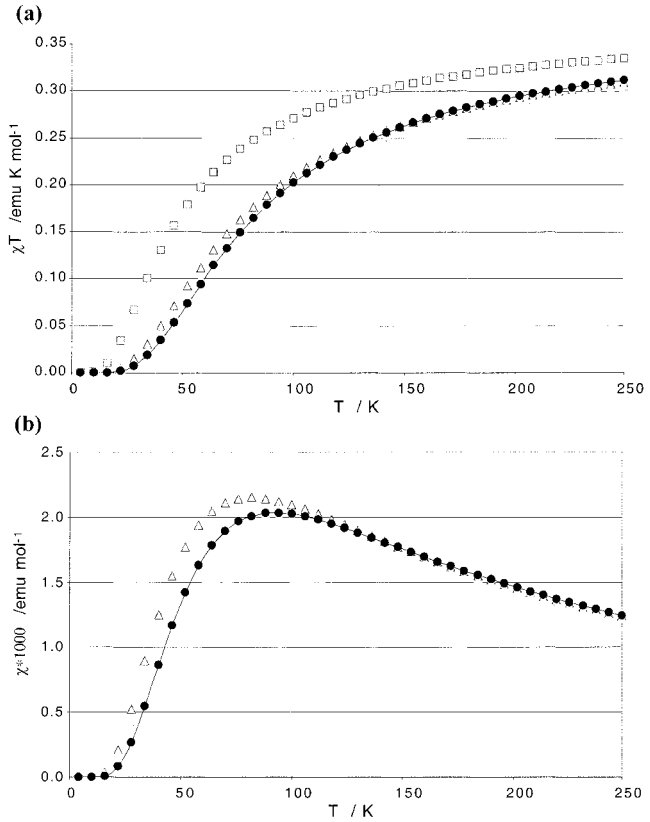

Figure 7. (a) $\chi T(T)$ using the 2mbb minimal model (■) data after applying a scaling factor of 1.6 (△) or 1.7 (▲) to the 2mbb model. (b) $\chi(T)$ with 1.6 (△) and 1.7 (▲) scaling factors. The experimental data are shown as (●).

minimal magnetic model space for WILVIW. By using the 1.7 scaling factor required to reproduce the experimental $\chi(T)$ data, the spin-gap becomes -84.7 cm^{-1} (spin-gap mean value times 1.7). We now compare this value to the Bleaney−Bowers fitting **J** parameter obtained by Awaga et al.,[41] which is the spin-gap for a two-level system (see discussion in Introduction). The difference between the experimentally fitted spin-gap $2\mathbf{J} = -102.8$ cm^{-1} and our simulated spin-gap -84.7 cm^{-1} is telling us that WILVIW cannot be described using a two-level model. This result is extremely important, because it implies that WILVIW is a many-level system (i.e., not only the two lowest energy levels are accessible). It follows that the energy levels introduced in the expression of $\chi(T)$ cannot be truncated after the first excited state (as the energy spectrum for the above-mentioned target spaces indicates; see Supporting Information Figure S1). This conclusion is justified by the fact that the fitting expression for the experimental data (eq 11) requires the introduction of the empirical mean field θ parameter.

Finally, the sensitivity of the computation of $\chi(T)$ to the magnetic motif in terms of the relative magnitudes of the dimeric interactions J_1... J_4 values is tested to demonstrate that we are not getting the right answer accidentally. Supporting Information S.I shows two tests where the topography of the spin ladder motif with a set of J_{AB} different from the computed J_{1-4} values is used. Both tests are compared to the 2mbb model simulated data since it is known to be the minimal magnetic model space for WILVIW. These tests enable us to conclude that the computation of $\chi(T)$ is highly sensitive to the magnetic motif in terms of the relative dimeric interactions. Thus, we are not getting the right answer accidentally, since by using the wrong set of dimeric interactions in the magnetic motif the simulated $\chi(T)$ values cannot reproduce the experimental data even qualitatively.

TABLE 2: Unrestricted DFT Broken Symmetry UB3LYP/6-31+G(d) Results for Each Candidate J_i ($i = 1-7$ Listed as O···O Distance Increases) for TOLKEK[a]

candidate i	d_i(O···O)/Å	J_i/cm^{-1}	J_i ordering
d1	3.80 (2)	−7.26	J_1
d2	4.27	+1.54	J_2
d3	4.65	+0.22	J_4
d4	4.79	+0.24	J_3
d5	6.12	−0.13	J_5
d6	6.22	< |0.05|	
d7	7.01	< |0.05|	

[a] The fourth column in Table 2 gives the ordering of the five non-negligible dimeric interactions $J_1 \cdots J_5$ from strongest to weakest dimeric interaction.

In summary, the analysis of the packing of the crystal, together with the computed dimeric interaction J_{AB} values, gives the magnetic picture of WILVIW at a microscopic level. The magnetic structure of this crystal is a two-dimensional layer, and its three-dimensional magnetic packing consists of a stack of parallel noninteracting two-dimensional layers. This microscopic magnetic picture is consistent with WILVIW being experimentally a low-dimensional antiferromagnet. The two-dimensional layer magnetic structure consists of weakly interacting antiferromagnetic spin ladder motifs. Several independent tests have proven that the minimal model capable of reproducing the macroscopic $\chi(T)$ values for WILVIW is a two-rung model (2mbb) with a 1.7 scaling factor, where a rung is considered the magnetic building block of this crystal. The two-rung 2mbb model contains microscopic information on the largest magnetic interactions J_1 and J_2. In addition, WILVIW has been found to behave as a many energy level system, and consequently, a spin-gap model—such as a pure Bleaney−Bowers equation[15]—cannot describe the magnetism of this crystal. This fact is in agreement with the fitting expression for the experimental data (eq 11), which requires the introduction of the empirical mean field θ parameter.[41]

TOLKEK. TOLKEK (α-2-hydroNN; for radical, see Scheme 2) crystallizes into the $P2_1/n$ space group ($a = 11.879$ Å, $b = 11.611$ Å, $c = 6.332$ Å, $\beta = 104.48°$, $Z = 4$) with four radicals per unit cell. TOLKEK behaves as an antiferromagnet[42] whose experimental magnetic susceptibility data have been fitted to a "pure" Bleaney−Bowers expression with $\mathbf{J}/k_B = -11.2$K (-7.8 cm^{-1}) and C=0.5 emu K mol^{-1}

$$\chi = \frac{C}{T}\frac{3}{3 + \exp(-2\mathbf{J}/k_B T)}\ [\text{emu mol}^{-1}] \qquad (12)$$

In this section, we will discuss the main results obtained for TOLKEK following the four-step prescription we propose in this paper. The analysis of the crystal packing in terms of O···O distances between ONCNO groups that are shorter than 7.4 Å suggests seven dimeric interactions, which must be computed. Table 2 shows the computed J_{AB} for d1−d7 pairs of radicals, which are listed as shortest O···O distance increases [for d1−d7 dimers see Supporting Information Figure S2]. Only five dimeric interactions are magnetically important and will contribute to the macroscopic magnetism of the crystal. The fourth column in Table 2 gives the ordering of $J_1 \cdots J_5$ relative to the strongest dimeric interaction.

We can now identify the magnetic building block, magnetic motif, and magnetic structure for TOLKEK. The magnetic building block is a dimer defined by the largest J_{AB} dimeric interaction ($J_1 = -7.26$ cm^{-1}). The extension of the magnetic

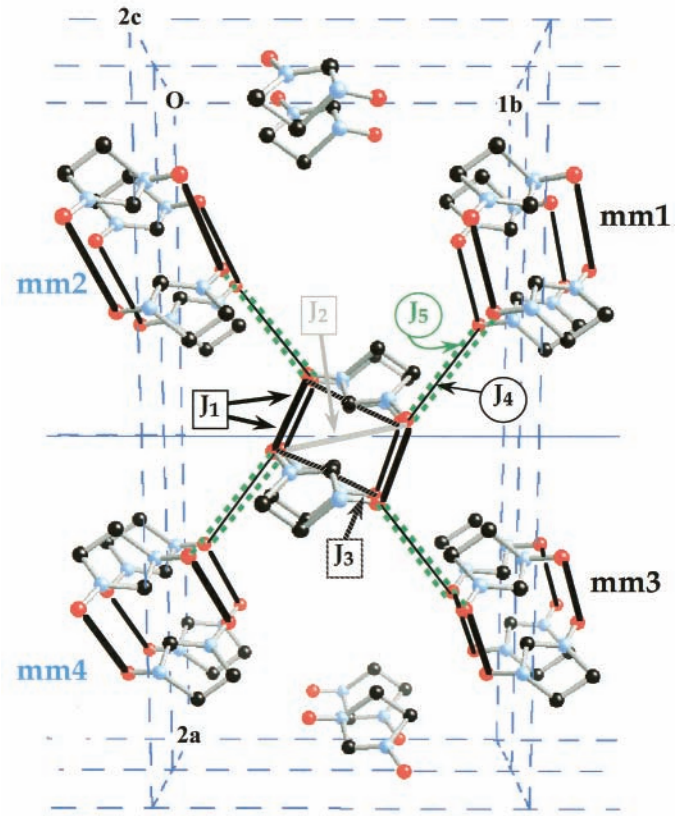

Figure 8. Two crystallographic cells for TOLKEK (only the imidazolyl ring is plotted, hydrogen atom and methyl groups are omitted). In the center of the figure, there are four TOLKEK radicals forming a spin ladder (J_1-J_3 are schematically drawn as a line connecting the shortest O···O distance between pairs of radicals) along the *c* crystallographic axis. Each spin ladder defined by J_1-J_3 interacts weakly with other four surrounding spin ladders (mm1−mm4) through J_4-J_5 along the *ab* axes.

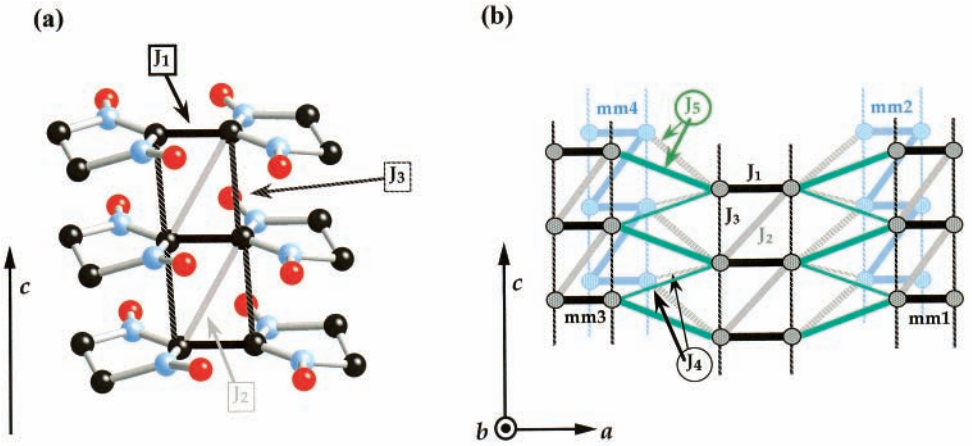

Figure 9. (a) Spin ladder motif shown along the *c* crystallographic axis (only the imidazolyl ring is plotted; hydrogen atom and methyl groups are omitted). The α-C atoms are connected instead of oxygen atoms for a better realization of the spin ladder magnetic motif. (b) Diagrammatic representation of the five spin ladders shown in Figure 8 (reference and mm1−mm4; each radical is replaced by a point site).

building block along the *c* axis through J_2-J_3 defines a spin ladder motif. Figure 8 shows two crystallographic cells for TOLKEK (only the imidazolyl ring is plotted, hydrogen atom and methyl groups are omitted). In the center of the figure, there are four TOLKEK radicals forming a spin ladder (J_1-J_3 are schematically drawn as a line connecting the shortest O···O distance between pairs of radicals) along the *c* crystallographic axis. This spin ladder along *c* is shown more clearly in Figure 9a, where α-C atoms are connected instead of oxygen atoms for a better realization of the magnetic motif. Each spin ladder defined by J_1-J_3 interacts weakly with other four surrounding spin ladders (mm1-mm4 in Figure 8) through J_4-J_5 along *ab* axes. Figure 9b is the diagrammatic representation of the five spin ladders shown in Figure 8 (each radical is replaced by a point site). The full magnetic structure for TOLKEK is then weakly three-dimensional due to the interaction between spin ladder motifs.

The convergence of the macroscopic susceptibility $\chi(T)$ is next studied in terms of increasing the number of magnetic building blocks (rung, mbb) along the *c* axis for a spin ladder (2mbb−4mbb) and then along *ab* axes to simulate five interacting spin ladders (see Figure 9b). Figure 10 demonstrates the very rapid convergence on $\chi(T)$ at high temperatures irrespective of the size of the model being used. In this figure the low-temperature region is also shown. It is clear that even at very low temperatures all models have a good convergence on $\chi(T)$

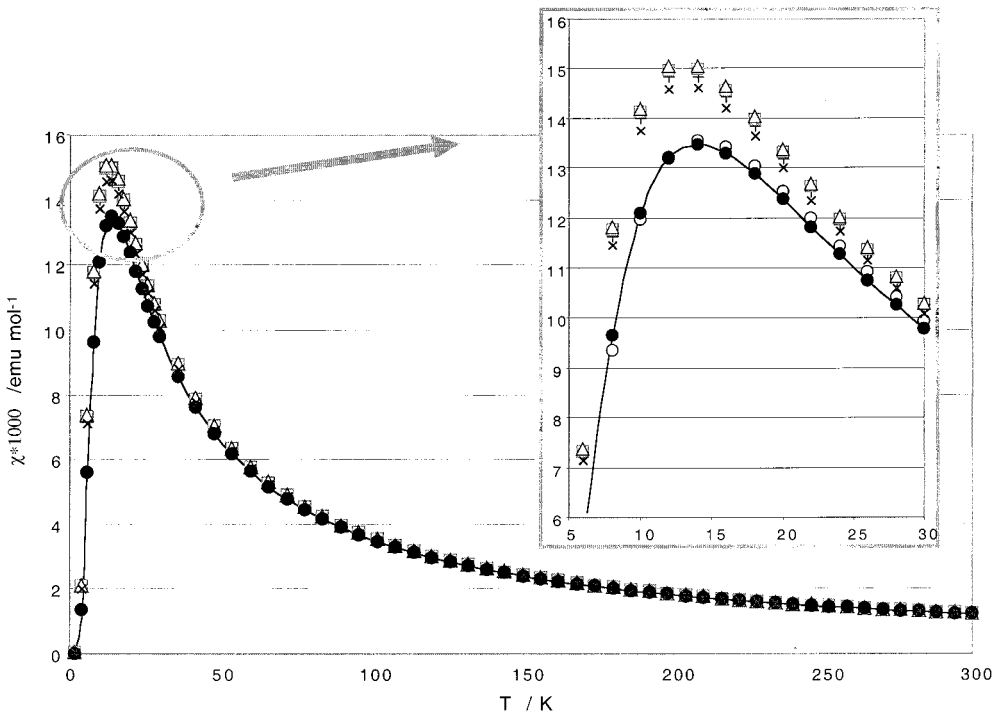

Figure 10. Simulated $\chi(T)$ results for TOLKEK using models for two (+), three (□), and four (△) magnetic building blocks (mbb) along the *c* axis for an isolated spin ladder, as well as along *ab* axes for a five spin ladder model (×) (see Figure 9b for diagrammatic view). In the inset, the low-temperature region is shown. A scaling factor of 1.1 applied to the 2mbb model (○) is required to reproduce the experimental $\chi(T)$ data (●).

(notice there is a slight improvement when we account for the inter-spin ladder dimeric interactions with a five spin ladder model, see Figure 9b). These results show that the 2mbb model is the minimal model of the magnetic motif, i.e., provides the minimal magnetic model space for TOLKEK.

Next, the discrepancy between simulated and experimental data in Figure 10 is taken into account. In this case, a scaling factor of only 1.1 applied to all J_{AB}'s of the 2mbb minimal model is required to reproduce the experimental $\chi(T)$ data (Figure 10). TOLKEK has a hydrogen H atom as R substituent attached to the α-C of the NN group (see Scheme 2). Thus, TOLKEK will have almost negligible three- or four-body cooperative exchange effects to account for, arising from the H atom substituent, in contrast to WILVIW that has a pyridinium ring.

Although we have demonstrated a 2mbb spin ladder model with three dimeric interactions J_{1-3} is the minimal magnetic model for TOLKEK, one should point out that J_3 is much smaller than J_1 and J_2. Therefore, this implies that the minimal model of the magnetic motif could even be a linear chain with two dimeric interactions J_{1-2} (instead of being a spin ladder motif; see Figure 9a). This simplification has been confirmed by tests using a linear chain with J_1 and J_2 instead of a spin ladder model as target space. All simulated results converge to those obtained with a four-site linear chain minimal model [Supporting Information Figure S3].

For TOLKEK, the computed spin-gap using all nonnegligible microscopic J_{AB} in the crystal for all different spin ladder motif target spaces (or linear chain motifs) has a mean value of -12.5 ± 3.5 cm^{-1} [Supporting Information Table S2]. The spin-gap for each individual target space decreases as the size of the target space increases, but the projected spin-gap is kept constant [see arrows for projected singlet and triplet states in Supporting Information Figure S4]. This result justifies once again the choice of the 2mbb spin ladder (or four-site linear chain) as representing the minimal magnetic model space for TOLKEK. By using the 1.1 scaling factor required to reproduce the experimental $\chi(T)$ data, the spin-gap becomes -13.8 cm^{-1} (spin-gap mean value times 1.1). We now compare this value to the Bleaney−Bowers (eq 12) **J** parameter obtained experimentally.[42] The agreement between experimentally fitted spin-gap $2\mathbf{J} = -15.6$ cm^{-1} and our "simulated" spin-gap -13.8 cm^{-1} tells that TOLKEK can be described using a two-level model.

Hosokoshi et al.[42] have suggested that the main magnetically important dimeric interactions are those with O···O distance of 3.80 and 4.27 Å (J_1 and J_2 respectively in Table 2). However, the authors assumed that only one of these interactions would contribute to the magnetism of TOLKEK. They identified the Bleaney−Bowers **J** parameter with an "actual" single dimeric interaction instead of being the singlet−triplet spin energy gap. However, the computed values obtained for J_1 (-7.26 cm^{-1}) and J_2 ($+1.54$ cm^{-1}) at UB3LYP/6-31+G(d) are not negligible and are in agreement with a two-level model for TOLKEK (as discussed above).

To summarize, we have shown that in order to give the correct physical interpretation to the microscopic magnetic paths in TOLKEK, it is absolutely essential to take into account all nonnegligible microscopic dimeric interactions J_{AB}. The magnetic structure of this crystal is three-dimensional and consists of weakly interacting spin ladders (or linear chains) as a magnetic motif. For TOLKEK, a 2mbb spin ladder (or four-site linear chain) minimal model with three (or two) dimeric interactions is capable of reproducing the experimental $\chi(T)$ data with a 1.1 scaling factor. In addition, we have proved that a minimal model with two or more J_{AB} interactions is not in contradiction with the system being described by a two-level model.

KAXHAS. Finally, we will discuss KAXHAS, the first bulk purely organic ferromagnet ever.[2] KAXHAS (*β-p*-nitrophenylNN; for radical, see Scheme 2) crystallizes into the orthorhombic F2dd space group ($a = 12.347$ Å, $b = 19.364$ Å, $c = 10.971$ Å, $Z = 8$) with eight radicals per unit cell. The

TABLE 3: Unrestricted DFT Broken Symmetry UB3LYP/6-31+G(d) Results for the Four Candidates (d1−d4 listed as O···O Distance Increases) for KAXHAS[a]

candidate *i*	d_i(O···O)/Å	J_i/cm^{-1}	J_i ordering
d1	5.35	+0.62	J_1
d2	6.43	+0.18	J_2
d3	6.73	< |0.05|	
d4	6.90	< |0.05|	

[a] The fourth column refers to the ordering of J_1 and J_2 from strongest to weakest dimeric interaction.

experimental magnetic susceptibility data for this crystal were fitted to a Curie−Weiss expression with $\theta = 1.2$ K (0.84 cm^{-1}) and $C = 0.376$ emu K mol^{-1} in the temperature range between 4 and 300 K

$$\chi = \frac{C}{T-\theta}\ [\text{emu mol}^{-1}] \tag{13}$$

Let us start the discussion for KAXHAS by analyzing the crystal packing in terms of O···O distances between ONCNO groups shorter than 7.4 Å.[18] The analysis suggests four pairs of radicals whose dimeric interaction should be computed [see Supporting Information Figure S5]. Table 3 shows that only two dimeric interactions ($J_1 > J_2$) are magnetically important and will contribute to the macroscopic magnetism of the crystal (d1−d4 listed in Table 3 as shortest O···O distance increases).

Figure 11 shows the nonnegligible J_1 and J_2 magnetic interactions between radical centers in terms of KAXHAS crystallographic unit cells (each radical is replaced by a point site; see Scheme 2). The packing of KAXHAS radicals is usually pictured as forming ABABA planes (*ac* crystallographic directions), as shown in Figure 11 taking the upper right unit cell as a reference (in the inset, *a*, *b*, *c* axes are given). Such a picture for the magnetic structure would suggest that J_2 is the driving force of the macroscopic magnetic interaction. However, J_1 is in fact the largest dimeric interaction, and the magnetic structure must be first analyzed in terms of this interaction. The analysis shows that the magnetic structure (and so the magnetic motif) is three-dimensional (thick lines in Figure 11), which is consistent with KAXHAS being experimentally a bulk ferromagnet.

For nonbulk magnets, one would proceed by identifying the magnetic building blocks of the magnetic motif defined by the dominant J_{AB} (e.g., WILVIW and TOLKEK). However, for bulk magnets, there are no isolated building blocks defined by the strongest J_{AB} and connected through weaker J_{AB} interactions as shown in Scheme 1. One must then identify the smallest repeating unit required in order to propagate the magnetic interactions in terms of J_{AB} along all spatial directions (J_1 for KAXHAS). For KAXHAS, we found that a 6-spin site, three-dimensional model (6s 3d, point sites labeled 1−6 are shown in Figure 11) is a suitable repeating unit (magnetic building block). In Figure 11, we show the propagation of the 6s 3d model required to fill the three-dimensional magnetic structure. There is a pure translation along the *b* crystallographic axis ($3d_z$) and two mixed translations along combinations of *a*/*c* axes ($3d_x$ and $3d_y$). These finite models are then used when applying the algebraic Heisenberg Hamiltonian (eq 7) to compute the microscopic energy levels required by the statistical mechanics definition of the magnetic susceptibility (eq 9).

Kinoshita [2c] has suggested, from the analysis of the crystal structure, that at least two kinds of exchange interactions (J and J') are expected to dominate the ferromagnetism of KAXHAS. Okumura et al.[45] estimated these interactions to be

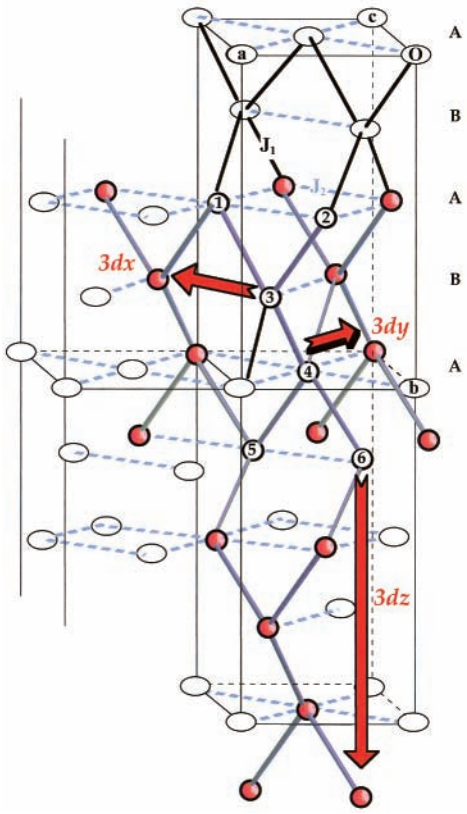

Figure 11. Nonnegligible J_1-J_2 magnetic interactions between radicals in terms of KAXHAS crystallographic cells (each radical is replaced by a point site, for formula see Scheme 2). According to J_2 (broken lines), the radicals pack forming ABABA planes (*ac* crystallographic directions) as shown in the upper right unit cell. According to J_1 (thick lines), the magnetic motif (and so the magnetic structure) is three-dimensional. The six-site three-dimensional magnetic building block (6s 3d) is given with point sites labeled 1−6. Inset in the figure, the propagation of the 6s 3d model required to fill the three-dimensional magnetic structure along the *b* axis ($3d_z$) and *a*/*c* axes ($3d_x$ and $3d_y$) is shown.

$J = +0.17$ cm^{-1} and $J' = +0.08$ cm^{-1} using the APUHF INDO method. Our computed values obtained at UB3LYP/6-31+G(d) are $J_1 = +0.62$ cm^{-1} and $J_2 = +0.18$ cm^{-1} to be compared to J and J' of Okumura,[45] respectively. There is a clear difference between these values as a consequence of a better description of the electron correlation at DFT level. However, the important point here is that different studies reach the same general conclusion about which exchange interactions J_1 and J_2 are magnetically important.

For KAXHAS, convergence on the magnetic susceptibility $\chi(T)$ has been explored by extending the 6-site three-dimensional (6s 3d) model along *a*, *b*, and *c* crystallographic directions ($3d_x$, $3d_y$, and $3d_z$, see Figure 11). Figure 12 shows that all simulated results for $\chi(T)$ converge at high temperatures, and even in the low-temperature region where $\chi T(T)$ is plotted in order to appreciate better the comparison among simulated data. Thus, the 6-spin site, three-dimensional (6s 3d) model is adequate to represent the magnetic structure for KAXHAS since it represents the minimal magnetic model space. To address the difference between experimental and simulated $\chi(T)$ data, a scaling factor of 1.8 is required (the R substituent attached to the α-C of the NN group is a phenyl group and the cooperative effects will be non negligible; see Scheme 2). This factor is in agreement with the 1.7 scaling factor obtained for WILVIW whose R substituent is a pyridinium ring.

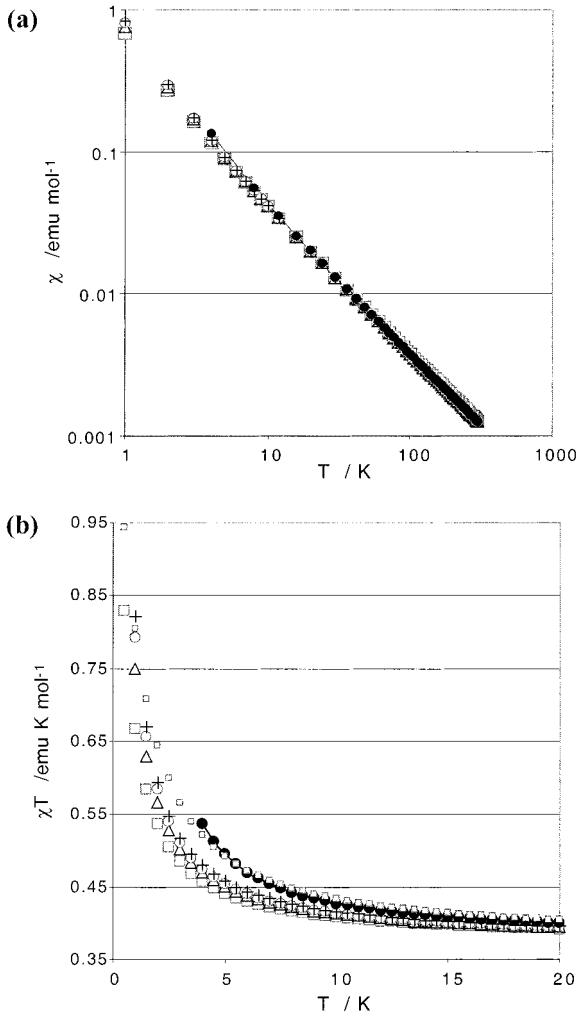

Figure 12. Simulated results for (a) $\chi(T)$ and (b) $\chi T(T)$ using the six-site three-dimensional 6s 3d model (■) and its extension $3d_x$ (△), $3d_y$ (○),and $3d_z$ (+). A scaling factor of 1.8 applied to the 6s 3d minimal model (□) is required to reproduce the experimental $\chi(T)$ data (●).

The experimental $\chi(T)$ data for KAXHAS have been fitted using the Curie−Weiss expression (15), where C is the Curie constant defined as

$$C = \frac{Ng^2\mu_B{}^2S(S+1)}{3k_B} \tag{14}$$

and θ is the Weiss temperature (or the mean field parameter) given by

$$\theta = \frac{zJS(S+1)}{3k_B} \tag{15}$$

In eqs 14 and 15, S is the spin of the magnetic center, g is the gyromagnetic factor, and N, μ_B, and k_B are Avogadro's number, Bohr magneton, and Boltzmann constant, respectively. Expression 13 is a modification of the Curie law to account for weak intermolecular interactions among radicals with non accessible excited states (large separation between ground and first excited states) and no first-order angular momentum. The interaction between magnetic centers is treated using molecular field theory with a magnetic Hamiltonian given by the Zeeman term and a perturbation $-zJ\langle S_z\rangle\hat{S}_z$ (for discussion see ref 46). According to this theory,[47] a given magnetic center interacts with strength J (pair interaction) with a number z of nearest neighbor centers in the crystal lattice. Thus, a given magnetic center feels the mean field $\langle S_z\rangle$ created by its z nearest neighbors. When using the mean field perturbation in the statistical mechanics $\chi(T)$ eq 9 for a one-level model (radical) system with transition between states with spin $-1/2$ and $1/2$, one can derive the Curie−Weiss expression (eq 13) and a higher order correction [for derivation, see Supporting Information S.II]

$$\chi = \frac{C}{T-\theta} - \frac{C}{2}\frac{T}{(T-\theta)^2} \tag{16}$$

Note that the C and θ values obtained in eq 16 correspond to replacing $S = 1/2$ in eqs 14 and 15. Let us now compare the value one would obtain for the mean intermolecular interactions J (using eq 15) to the computed dimeric interaction J_{AB} values for KAXHAS.

From Figure 11, one can see that each point site (radical) interacts through J_1 with four nearest neighbors and through J_2 with other four. Thus taking $z = 4$, J is $+0.83$ cm^{-1}, and if $z = 8$, then J is $+0.42$ cm^{-1}. Comparing these values to J_1 ($+0.62$ cm^{-1}), we realize that $J(z{=}4)$ is too large because it does not account for J_2-type interactions and $J(z{=}8)$ is too small since it does not distinguish between J_1 and J_2 interactions. Therefore, a Curie−Weiss expression has limited value for understanding the microscopic picture of a magnetic center interacting with its neighbors due to the fact that this methodology averages all magnetic interactions. Moreover, we must stress that the energy spectra for KAXHAS using any of the target spaces (6s 3d, $3d_x$, $3d_y$, and $3d_z$) shows that all the energy levels are accessible, not just the ground state [Supporting Information Figure S6]. It follows that for such a ferromagnetic example, there is no way to justify the application of the one-level Curie−Weiss model (nor a two-level Bleaney−Bowers model).

After correctly reproducing the $\chi(T)$ experimental data, we have simulated the heat capacity $C_p(T)$ data for KAXHAS by using the 6s 3d minimal model and extending it along *a*, *b*, and *c* crystallographic directions ($3d_x$, $3d_y$, and $3d_z$; see Figure 11). Statistical mechanics provides an expression for $C_p(T)$ (eq 10) in terms of microscopic energy levels (the units for C_p are J mol^{-1} K^{-1}). The experimental heat capacity has a sharp peak at the ferromagnetic transition temperature T_C of 0.6 K, corresponding to a three-dimensional (second order) magnetic phase transition. Figure 13 shows the simulated $C_p(T)$ data for KAXHAS. The maximum temperature for all models gives a critical temperature of 0.45K, which is in qualitative agreement with the experimental ferromagnetic transition temperature of 0.60 K. Obviously, Figure 13 does not show the typical λ-shape of $C_p(T)$ since we are not using the crystal but a finite small model. However, one can see that when increasing the number of sites (from 6 to 12) in the model the curve does get sharper.

According to this study, a 6-site and two exchange coupling constant minimal model (6s 3d) is the most adequate to give a good description to the microscopic magnetic paths for KAXHAS. This three-dimensional ferromagnetic building block (repeating unit) defines a three-dimensional magnetic structure, which is consistent with KAXHAS being a bulk ferromagnet. By using the microscopic magnetic information of the 6-site and two dimeric interaction model, one is able to describe the heat capacity behavior C_p as well as the magnetic susceptibility χ as a function of temperature, and estimate the ferromagnetic transition critical temperature. It has been shown that neither a one-level Curie−Weiss nor a two-level Bleaney−Bowers models is consistent with the energy spectra of KAXHAS [as shown in Supporting Information Figure S6].

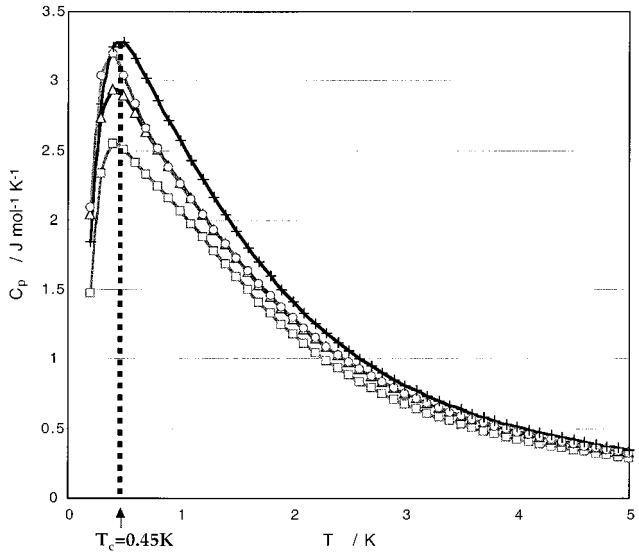

Figure 13. Simulated $C_p(T)$ data for KAXHAS using the six-site three-dimensional 6s 3d minimal model (■) and its extension $3d_x$ (△), $3d_y$ (○),and $3d_z$ (+).

Conclusions

The method we have used in this work to study the magnetism in molecular crystals is essentially a numerical approach. We have simulated the magnetic susceptibility $\chi(T)$ (eq 9)—and heat capacity $C_p(T)$ (eq 10)—using the energy levels computed with an algebraic Heisenberg Hamiltonian (eq 7) parametrized with J_{AB} (eq 6), which have been computed using DFT. Once the magnetic susceptibility data are computed, it can be compared to the experimental $\chi(T)$ data. The computed J_{AB} interactions are essential not only in the parametrization procedure, but also in the basic definition of the microscopic magnetic structure of the molecular crystal (e.g., spin ladder, etc.). Using this numerical approach, a very rapid convergence on the magnetic susceptibility $\chi(T)$ is obtained. Thus, simple models (i.e., small number of radical sites) and a linear scaling of the previously computed J_{AB} proves to be adequate. Therefore, we have shown that we can directly relate the microscopic magnetic information (magnetic structure, magnetic motif and magnetic building block defined by J_{AB} dimeric interactions) to the macroscopic properties of a crystal (e.g., magnetic susceptibility, heat capacity, etc.). The four-step prescription we propose has been shown to reproduce the experimental data and to rationalize the bulk ferromagnetism of KAXHAS and the antiferromagnetism of WILVIW and TOLKEK.

In the literature, one can distinguish between models for fitting the experimental magnetic susceptibility $\chi(T)$ data depending on whether they (1) make explicit reference to microscopic data (e.g., J_{AB}) or (2) are based on two-level spin-gap-type models (e.g., Bleaney−Bowers[15]), one-level Curie−Weiss[46] model, etc., which do not contain microscopic information explicitly. Our computations rationalize why a spin-gap model (i.e., Bleaney−Bowers) is suitable for reproducing the experimental $\chi(T)$ data of some antiferromagnetic crystals (e.g., TOLKEK). However, such a model only provides a mechanism for fitting the experimental data. It cannot provide understanding about the microscopic picture of the interacting magnetic centers (i.e., J_{AB}). For bulk ferromagnets, our computations suggest that neither a two-level Bleaney−Bowers nor a Curie−Weiss model should be used, since the energy spectrum for such a crystals shows an almost continuum of levels.

In contrast to models such as Bleaney−Bowers,[15] other models that contain microscopic data have been proposed to fit the experimental data using an analytical function of the microscopic J_{AB}, etc. parameters for the magnetic susceptibility $\chi(T)$.[13] The specific analytical expression for $\chi(T)$ depends on using a model (linear chain, spin ladder, etc.) containing a series of microscopic parameters (e.g., J_{AB}, D, g, etc.). The model itself is a hypothesis since the actual magnetic structure of the crystal (J_{AB}) is not known a priori. If the experimental data can be fitted with such analytical expressions, the resulting fitting parameters do give indeed information about the microscopic structure of the crystal (J_{AB}). For instance, from our computations, we demonstrate that in WILVIW crystal an analytical function of J_{AB} based on a spin ladder model is essentially correct. The problem is that, often, more than one analytical model may fit the experimental $\chi(T)$ data sensibly.

Our computations suggest a general strategy for the description of the macroscopic magnetism in molecular crystals taking into account the microscopic information. Our numerical approach demonstrates rapid convergence on $\chi(T)$. Thus, a small number of radical sites interacting in the correct magnetic motif, after linear scaling the computed J_{AB} interactions, has been demonstrated to be sufficient to reproduce qualitatively the experimental data. It has been shown that the topography of the J_{AB} and the correct relative magnitudes and sign of the computed J_{AB} are the essential elements of the magnetic structure. Therefore, although a simple linear scaling has been adequate to reproduce qualitatively the experimental $\chi(T)$ data, we could refine the microscopic J_{AB} values using a general nonlinear fitting to the actual experimental $\chi(T)$ data.

Acknowledgment. This project was supported by EPSRC (UK) under Grant GR/M86750 (ROPA).

Supporting Information Available: Figures of energy spectra vs spin number, dimer arrangement, and magnetic susceptibility; tables of spin-gap data; schemes of the sensitivity of the computation of $\chi(T)$ to the magnetic motif, derivation of the Curie−Weiss expression, computation of the energy, and cartesian coordinates. This material is available free of charge via the Internet at http://pubs.acs.org.

References and Notes

(1) (a) Kahn, O. *Molecular Magnetism*; VCH Publishers: New York, 1993. (b) Miller, J. S.; Epstein, A. J. *Angew. Chem., Int. Ed. Engl.* **1994**, *33*, 385. (c) Coronado, E., Delhaès, P., Gatteschi, D., Miller, J. S., Eds. In *Molecular Magnetism: From Molecular Assemblies to the Devices*; NATO ASI Series E; Kluwer Acad. Publishers: Dordrecht, 1996; Vol 321 and references therein. (d) All the *Proceedings of the International Conference on Molecule-Based Magnets*, the latest being: Kahn, O., *Mol. Cryst. Liq. Cryst.* **1999**, *334*, 1−712; *335*, 1−706.

(2) (a) Tamura, M.; Nakazawa, Y.; Shiomi, D.; Nozawa, K.; Hosokoshi, Y.; Ishikawa, M.; Takahashi, M.; Kinoshita, M. *Chem. Phys. Lett.* **1991**, *186*, 401. (b) Nakazawa, Y.; Tamura, M.; Shirakawa, N.; Shiomi, D.; Takahashi, M.; Kinoshita, M.; Ishikawa, M. *Phys. Rev. B* **1992**, *46*, 8906. (c) Kinoshita, M. *Jpn. J. Appl. Phys.* **1994**, *33*, 5718.

(3) Allemand, P.-M.; Khemani, K. C.; Koch, A.; Wudl, F.; Holczer, K.; Donovan, S.; Gruner, G.; Thompson, J. D. *Science* **1991**, *253*, 301.

(4) For examples of purely organic nitronyl nitroxide ferromagnetic crystals, see: (a) Awaga, K.; Inabe, T.; Maruyama, Y. *Chem. Phys. Lett.* **1992**, *190*, 349. (b) Sugano, T.; Tamura, M.; Kinoshita, M.; Sakai, Y.; Ohashi, Y. *Chem. Phys. Lett.* **1992**, *200*, 235. (c) Hernandez, E.; Mas, M.; Molins, E.; Rovira, C.; Veciana, J. *Angew. Chem., Int. Ed. Engl.* **1993**, *32*, 882. (d) de Panthou, F. L.; Luneau, D.; Laugier, J.; Rey, P. *J. Am. Chem. Soc.* **1993**, *115*, 9095. (e) Wang, H.; Zhang, D.; Wan, M.; Zhu, D. *Solid State Commun.* **1993**, *85*, 685. (f) Angeloni, L.; Caneschi, A.; David, L.; Fabretti, A.; Ferraro, F.; Gatteschi, D.; le Lirzin, A.; Sessoli, R. *J. Mater. Chem.* **1994**, *4*, 1047. (g) Hosokoshi, Y.; Tamura, M.; Kinoshita, M.; Sawa, H.; Kato, R.; Fujiwara, Y.; Ueda, Y. *J. Mater. Chem.* **1994**, *4*, 1219. (h) Caneschi, A.; Ferraro, F.; Gatteschi, D.; le Lirzin, A.; Rentschler, E. *Inorg. Chim. Acta* **1995**, *235* 159. (i) Cirujeda, J.; Mas, M.; Molins, E.; de Panthou, F. L.; Laugier, J.; Park, J. G.; Paulsen, C.; Rey, P.; Rovira, C.; Veciana, J. *J. Chem. Soc. Chem. Commun.* **1995**, 709. (j) Hosokoshi, Y.; Tamura, M.;

Sawa, H.; Kato, R.; Kinoshita, M. *J. Mater. Chem.* **1995**, *5*, 41. (k) Akita, T.; Mazaki, Y.; Kobayashi, K.; Koga, N.; Iwamura, H. *J. Org. Chem.* **1995**, *60*, 2092. (l) Lang, A.; Pei, Y.; Ouahab, L.; Kahn, O. *Adv. Mater.* **1996**, *8*, 60. (m) Matsushita, M. M.; Izuoka, A.; Sugawara, T.; Kobayashi, T.; Wada, N.; Takeda, N.; Ishikawa, M. *J. Am. Chem. Soc.* **1997**, *119*, 4369.

(5) (a) Carlin, R. L. *Magnetochemistry*; Springer-Verlag Berlin Heidelberg, 1986. (b) Ref 1a. (c) Boca, R. Theoretical Foundations of Molecular Magnetism. *Current Methods in Inorganic Chemistry*; Elsevier Science: Amsterdam, 1999; Vol. 1.

(6) (a) McConnell, H. M. *J. Chem. Phys.* **1963**, *39*, 1910. (b) McConnell, H. M. *Proc. Robert A. Welch Found. Conf. Chem. Res.* **1967**, *11*, 144. (c) Deumal, M.; Novoa, J. J.; Bearpark, M. J.; Celani, P.; Olivucci, M.; Robb, M. A. *J. Phys. Chem. A* **1998**, *102*, 8404. (d) Kollmar, C.; Kahn, O. *Acc. Chem. Res.* **1993**, *26*, 259.

(7) (a) Guihéry, N.; Malrieu, J. P.; Maynau, D.; Wind, P. *Mol. Phys.* **1998**, *96*, 209. (b) Wind, P.; Guihéry, N.; Malrieu, J. P. *Phys. Rev. B* **1999**, *59*, 2556. (c) Illas, F.; Moreira, I. P. R.; de Graaf, C.; Castell, O.; Casanovas, J. *Phys. Rev. B* **1997**, *56*, 5069. (d) Moreira, I. P. R.; Illas, F.; Calzado, C. J.; Sanz, J. F.; Malrieu, J. P.; Ben Amor, N.; Maynau, D. *Phys. Rev. B* **1999**, *59*, R6593. (e) Barone, V.; Bencini, A.; diMatteo, A. *J. Am. Chem. Soc.* **1997**, *119*, 10831.

(8) (a) Towler, M. D.; Dovesi, R.; Saunders: V. R. *Phys. Rev. B* **1995**, *52*, 10150. (b) Bencini, A.; Totti, F.; Daul, C. A.; Doclo, K.; Fantucci, P.; Barone, V. *Inorg. Chem.* **1997**, *36*, 5022. (c) Bencini, A.; Ciofini, I.; Giannasi, E.; Daul, C. A.; Doclo, K. *Inorg. Chem.* **1998**, *37*, 3719. (d) Ruiz, E.; Cano, J.; Alvarez, S.; Alemany, P. *J. Comput. Chem.* **1999**, *20*, 1391. (e) Mitani, M.; Mori, H.; Takano, Y.; Yamaki, D.; Yoshioka, Y.; Yamaguchi, K. *J. Chem. Phys.* **2000**, *113*, 4035. (f) Blanchet-Boiteux, C.; Mouesca, J. M. *J. Phys. Chem. A* **2000**, *104*, 2091. (g) Rodriguez-Fortea, A.; Alemany, P.; Alvarez, S.; Ruiz, E. *Chem. Eur. J.* **2001**, *7*, 627.

(9) For a review on quantum-mechanical periodic programs, see Pisani, C. *J. Mol. Struct. (THEOCHEM)* **1999**, *463*, 125 and references therein.

(10) (a) Borrás-Almenar, J. J.; Clemente-Juan, J. M.; Coronado, E.; Tsukerblat, B. S. *Inorg. Chem.* **1999**, *38*, 6081. (b) Borrás-Almenar, J. J.; Clemente-Juan, J. M.; Coronado, E.; Tsukerblat, B. S. *J. Comput. Chem.* **2001**, *22*, 985.

(11) Fink, K.; Wang, C.; Staemmler, V. *Inorg. Chem.* **1999**, *38*, 3847.

(12) Hellberg, C. S.; Pickett, W. E.; Boyer, L. L.; Stokes, H. T.; Mehl, M. J. *J. Phys. Soc. Jpn.* **1999**, *68*, 3489.

(13) (a) Baker, G. A.; Rushbrooke, G. S.; Gilbert, H. E. *Phys. Rev. A* **1964**, *135*, 1272. (b) Duffy, W.; Barr, K. P. *Phys. Rev.* **1968**, *165*, 647. (c) Diederix, K. M.; Blöte, H. W. J.; Groen, J. P.; Klaassen, T. O.; Poulis, N. J. *Phys. Rev. B* **1979**, *19*, 420. (d) Hall, J. W.; Marsh, W. E.; Weller, R. R.; Hatfield, W. E. *Inorg. Chem.* **1981**, *20*, 1033. (e) Hatfield, W. E. *J. Appl. Phys.* **1981**, *52*, 1985. (f) Coronado, E.; Drillon, M.; Fuertes, A.; Beltran, D.; Mosset, A.; Galy, J. *J. Am. Chem. Soc.* **1986**, *108*, 900. (g) Barnes, T.; Dagotto, E.; Riera, J.; Swanson, E. S. *Phys. Rev. B* **1993**, *47*, 3196. (h) Borrás-Almenar, J. J.; Coronado, E.; Curely, J.; Georges, R.; Gianduzzo, J. C. *Inorg. Chem.* **1994**, *33*, 5171. (i) Barnes, T.; Riera, J. *Phys. Rev. B* **1994**, *50*, 6817. (j) Borrás-Almenar, J. J.; Clemente-Juan, J. M.; Coronado, E.; Lloret, F. *Chem. Phys. Lett.* **1997**, *275*, 79. (k) Barnes, T.; Riera, J.; Tennant, D. A. *Phys. Rev. B* **1999**, *59*, 11384.

(14) (a) Gatteschi, D.; Pardi, L. *Gazz. Chim. It.* **1993**, *123*, 231. (b) Shiomi, D.; Tamura, M.; Katori, H. A.; Goto, T.; Hayashi, A.; Ueda, Y.; Sawa, H.; Kato, R.; Kinoshita, M. *J. Mater. Chem.* **1994**, *4*, 915. (c) Castro, I.; Calatayud, M. L.; Sletten, J.; Lloret, F.; Cano, J.; Julve, M.; Seitz, G.; Mann, K. *Inorg. Chem.* **1999**, *38*, 4680. (d) Gutierrez, L.; Alzuet, G.; Real, J. A.; Cano, J.; Borras, J.; Castinyeiras, A. *Inorg. Chem.* **2000**, *39*, 3608.

(15) Bleaney, B.; Bowers, K. D. *Proc. R. Soc. London, Ser. A* **1952**, *214*, 451.

(16) An exact derivation can be found in: Boca, R. Theoretical Foundations of Molecular Magnetism. *Current Methods in Inorganic Chemistry*; Elsevier Science: Amsterdam, 1999; Vol. 1, Chapter 10, section 10.2.1, pp 620−621).

(17) For instance, see: Chandramouli, G. V. R.; Balagopalakrishna, C.; Rajasekharan, M. V.; Manoharan, P. T. *Comput. Chem.* **1996**, *20*, 353.

(18) (a) Herring, C. Direct Exchange between Well-Separated Atoms. In *Magnetism*; Rado, G. T., Suhl, H., Eds.; Academic Press: New York, 1966; Vol. IIB, p 5. (b) For nitronyl nitroxide NN crystals, a spin carrier intersite threshold ONCNO···ONCNO distance of 7.4 Å is chosen to ensure the identification of all potentially important magnetic interactions. This threshold distance comes from increasing by 1.00 Å the largest ONCNO···ONCNO distance between radicals (6.43 Å for KAXHAS[2]) with a nonnegligible computed magnetic J_{AB} interaction.

(19) (a) Deumal, M.; Cirujeda, J.; Veciana, J.; Novoa, J. J. *Adv. Mater.* **1998**, *10*, 1461. (b) Deumal, M.; Cirujeda, J.; Veciana, J.; Novoa, J. J. *Chem. Eur. J.* **1999**, *5*, 1631.

(20) Deumal, M.; Lafuente, P.; Mota, F.; Novoa, J. J. *Synth. Met.* **2001** (Award Symposium for J. S. Miller Issue).

(21) (a) Pisani, C.; Dovesi, R.; Roetti, C. *Hartree−Fock Ab Initio Treatment of Crystalline Systems*; Lecture Notes in Chemistry; Springer: Berlin, 1988; Vol. 48. (b) Roetti, C., Pisani, C., Eds. *Quantum-Mechanical Ab Initio Calculation of the Properties of Crystalline Materials*; Lecture Notes in Chemistry; Springer: Berlin, 1996; Vol.67, p 125. (c) Saunders, V. R.; Dovesi, R.; Roetti, C.; Causà, M.; Harrison, N. M.; Orlando, R.; Zicovich-Wilson, C. M. *CRYSTAL 98 User's Manual*; Università di Torino: Torino, Italy, 1998.

(22) For a discussion on unrestricted DFT with broken symmetry, see: (a) Noodlemann, L. *J. Chem. Phys.* **1981**, *74*, 5737. (b) Noodlemann, L.; Davidson, E. R. *Chem. Phys.* **1986**, *109*, 131. (c) Parr, R. G.; Yang, W. *Density-Functional Theory of Atoms and Molecules*; Oxford University Press: New York 1989. (d) Noodlemann, L.; Case, D. A. *Adv. Inorg. Chem.* **1992**, *38*, 423. (e) Noodlemann, L.; Peng, C. Y.; Case, D. A.; Mouesca, J. M. *Coord. Chem. Rev.* **1995**, *144*, 199. (f) Ruiz, E.; Alemany, P.; Alvarez, S.; Cano, J. *J. Am. Chem. Soc.* **1997**, *119*, 1297. (g) Caballol, R.; Castell, O.; Illas, F.; Moreira, I. D. R.; Malrieu, J. P. *J. Chem. Phys. A* **1997**, *101*, 7860. (h) Ref 8d. (i) Nagao, H.; Nishino, M.; Shigeta, Y.; Soda, T.; Kitagawa, Y.; Onishi, T.; Yoshioka, Y.; Yamaguchi, K. *Coord. Chem. Rev.* **2000**, *198*, 265. (j) Mouesca, J.-M. *J. Chem. Phys.* **2000**, *113*, 10505. (k) Illas, F.; Moreira, I. D. R.; de Graaf, C.; Barone, V. *Theor. Chem. Acc.* **2000**, *104*, 265.

(23) (a) Becke, A. D. *Phys. Rev. A* **1988**, *38*, 3098. (b) Lee, C.; Yang, W.; Parr, R. G. *Phys. Rev. B* **1988**, *37*, 785. (c) Becke, A. D. *J. Chem. Phys.* **1993**, *98*, 5648.

(24) 6-31+G(d) ≡ DZ basis set, including diffuse and polarization functions.

(25) Frisch, M. J.; Trucks, G. W.; Schlegel, H. B.; Scuseria, G. E.; Robb, M. A.; Cheeseman, J. R.; Zakrzewski, V. G.; Montgomery, J. A., Jr.; Stratmann, R. E.; Burant, J. C.; Dapprich, S.; Millam, J. M.; Daniels, A. D.; Kudin, K. N.; Strain, M. C.; Farkas, O.; Tomasi, J.; Barone, V.; Cossi, M.; Cammi, R.; Mennucci, B.; Pomelli, C.; Adamo, C.; Clifford, S.; Ochterski, J.; Petersson, G. A.; Ayala, P. Y.; Cui, Q.; Morokuma, K.; Malick, D. K.; Rabuck, A. D.; Raghavachari, K.; Foresman, J. B.; Cioslowski, J.; Ortiz, J. V.; Stefanov, B. B.; Liu, G.; Liashenko, A.; Piskorz, P.; Komaromi, I.; Gomperts, R.; Martin, R. L.; Fox, D. J.; Keith, T.; Al-Laham, M. A.; Peng, C. Y.; Nanayakkara, A.; Gonzalez, C.; Challacombe, M.; Gill, P. M. W.; Johnson, B. G.; Chen, W.; Wong, M. W.; Andres, J. L.; Head-Gordon, M.; Replogle, E. S.; Pople, J. A. *Gaussian 98*; Gaussian, Inc.: Pittsburgh, PA, 1998.

(26) (a) Castell, O.; Caballol, R.; Garcia, V. M.; Handrick, K. *Inorg. Chem.* **1996**, *35*, 1609. (b) Castell, O.; Caballol, R. *Inorg. Chem.* **1999**, *38*, 668. (c) Ref 11. (d) Kolczewski, C.; Fink, K.; Staemmler, V. *Int. J. Quantum Chem.* **2000**, *76*, 137. (e) Mitani, M.; Yamaki, D.; Takano, Y.; Kitagawa, Y.; Yoshioka, Y.; Yamaguchi, K. *J. Chem. Phys.* **2000**, *113*, 10486. (f) Cabrero, J.; Ben Amor, N.; de Graaf, C.; Illas, F.; Caballol, R. *J. Phys. Chem. A* **2000**, *104*, 9983.

(27) As an example, a molecular two-leg spin ladder is shown in Scheme 1c [for a recent review on spin ladders, see: Rovira, C. *Chem. Eur. J.* **2000**, *6*, 1723−1729]. If J_1 is the largest dimeric interaction, the spin ladder results from combining A−B dimer building blocks as rungs given by J_1 (Scheme 1a) connected through J_2 to form the side poles or legs of the "ladder". However, if J_2 is the largest one, then the magnetic motif results from the assembly of two one-dimensional chains (Scheme 1b) interacting through J_1.

(28) (a) Herring, C. Direct Exchange between Well-Separated Atoms. In *Magnetism*; Rado, G. T., Suhl, H., Eds.; Academic Press: New York, 1966; Vol. IIB, pp 1−181). (b) McWeeny, R.; Sutcliffe, B. T. *Methods of Molecular Quantum Mechanics*; Academic Press: New York, 1969.

(29) The Hamiltonian (eq 7) operates on a basis of N-fold tensor products consisting of products of N spins (either α or β for a system of doublets) in the crystal. For N electrons in N magnetic centers/orbitals, we have used Hartree Waller functions [Waller, I.; Hartree, D. R. *Proc. R. Soc. London, Ser. A* **1929**, *119*, 124] as the basis for the matrix representation of eq 7. The Hartree Waller functions are partly spin-adapted configurations, which are eigenfunctions of $\hat{S}_z$. The use of these functions simplifies the calculation by splitting the secular determinant of the Heisenberg Hamiltonian problem into two blocks. The spin antisymmetric/symmetric combinations (antisymmetric/symmetric Hartree Waller functions) will provide even ($S = 0$, 2, etc.)/odd ($S = 1$, 3, etc.) spin solutions, respectively.

(30) (a) Born, M.; von Karman, Th. *Phys. Z.* **1912**, *13*, 297. (b) Born, M.; von Karman, Th. *Phys. Z.* **1913**, *14*, 15. (c) Slater, J. C. *Quantum Theory of Matter*, 2nd ed.; McGraw-Hill: New York, 1968; pp 600−602. (d) Altmann, S. L. *Band Theory of Solids*; Clarendon Press: Oxford, 1991; p 8. (e) Refs 13c−f,h,j.

(31) (a) Bonner, J. C.; Fisher, M. E. *Phys. Rev. A* **1964**, *135*, 640−659 (see references therein for a hystorical review of treating chain/ring systems). (b) Kirtman, B.; Nilsson, W. B.; Palke, W. *Solid State Commun.* **1983**, *46*, 791. (c) Refs 13a−c,e,i.

(32) Bloch, C. *Nucl. Phys.* **1958**, *6*, 329.

(33) Malrieu, J. P.; Guihéry, N. *Phys. Rev. B* **2001**, *63*, 5110−5119. The authors formulate a renormalization-group procedure where the renormalized Hamiltonian is defined as a Bloch effective Hamiltonian. This procedure is based on the real-space renormalization-group (RSRG)

method: (a) Wilson, K. G. *Rev. Mod. Phys.* **1975**, *47*, 773. (b) White, S. R.; Noack, R. M. *Phys. Rev. Lett.* **1992**, *68*, 3487.

(34) Most of the magnetic measurements in ref 4 were performed using a SQUID magnetometer.

(35) See Kahn, O. *Molecular Magnetism*; VCH Publishers: New York, 1993; p 112 for same derivation applied to dinuclear compounds.

(36) Further, one must be careful since the magnetic susceptibility is sometimes expressed as a quantity per mole emu mol^{-1} (mole of either dimers or radicals), per unit volume, emu cm^{-3}, or per unit mass, emu kg^{-1}.

(37) (a) Ref 8a. (b) Orlando, R.; Dovesi, R.; Ugliengo, P.; Roetti, C.; Saunders, V. R. *Int. J. Inorg. Mater.* **1999**, *1*, 147. (c) Reinhardt, P.; Moreira, I. D. R.; de Graaf, C.; Dovesi, R.; Illas, F. *Chem. Phys. Lett.* **2000**, *319*, 625.

(38) Supporting Information S.III contains the results for the reverse process, i.e., the computation of energy values using the J_{AB} obtained from CRYSTAL[37c] to parametrize our algebraic Heisenberg Hamiltonian approach.

(39) (a) Trivedi, N.; Ceperley, D. M. *Phys. Rev. B* **1990**, *41*, 4552. (b) Runge, K. J. *Phys. Rev. B* **1992**, *45*, 12292. (c) Dagotto, E. *Rev. Mod. Phys.* **1994**, *66*, 763. (d) Cano-Boquera, J.; Journaux, Y. *Mol. Cryst. Liq. Cryst.* **1999**, *335*, 1397. (e) Korotin, M. A.; Elfimov, I. S.; Anisimov, V. I.; Troyer, M.; Khomskii, D. I. *Phys. Rev. Lett.* **1999**, *83*, 1387.

(40) (a) White, S. R. *Phys. Rev. B* **1993**, *48*, 10345. (b) White, S. R. *Phys. Rev. Lett.* **1992**, *69*, 2863. (c) White, S. R. *Phys. Rev. Lett.* **1996**, *77*, 3633−3636.

(41) Awaga, K.; Yamaguchi, A.; Okuno, T.; Inabe, T.; Nakamura, T.; Matsumoto, M.; Maruyama, Y. *J. Mater. Chem.* **1994**, *4*, 1377−1385.

(42) Hosokoshi, Y.; Tamura, M.; Nozawa, K.; Suzuki, S.; Kinoshita, M.; Sawa, H.; Kato, R. *Synth. Met.* **1995**, *71*, 1795−1796.

(43) Cambridge Crystallographic Structural Database (CCSD): (a) Allen, F. H.; Davies, J. E.; Galloy, J. J.; Johnson, O.; Kennard, O.; Macrae, C. F.; Watson, D. G. *J. Chem. Inf. Comput. Sci.* **1991**, *31*, 204. (b) Allen, F. H.; Kennard, O. *Chem. Des. Automation News* **1993**, *8*, 31

(44) 10−15% systematic error compared to FCI, DDCI (Novoa, J. J.; Caballol, R.; et al. Manuscript to be submitted).

(45) Okumura, M.; Mori, W.; Yamaguchi, K. *Mol. Cryst. Liq. Cryst.* **1993**, *232*, 35−44.

(46) For discussion on Curie−Weiss law, see: Kahn, O. *Molecular Magnetism*; VCH Publishers: New York, 1993; p 26. Boca, R. Theoretical Foundations of Molecular Magnetism. *Current Methods in Inorganic Chemistry*; Elsevier Science: Amsterdam, 1999; Vol. 1, p 535.

(47) For mean field theory, see: Kahn, O. *Molecular Magnetism*; VCH Publishers: New York, 1993; pp 26 and 131. Carlin, R. L. *Magnetochemistry*; Springer-Verlag Berlin Heidelberg, 1986; p 113. Boca, R. Theoretical Foundations of Molecular Magnetism. *Current Methods in Inorganic Chemistry*; Elsevier Science: Amsterdam, 1999; Vol. 1, p 355.